Influence of Mold Coating Wear on Heat Transfer Coefficient in Aluminum Permanent Molds

by

Sean Roorda

Submitted to the Faculty in partial fulfillment of the requirements for the degree of

Master's of Science

in

Material Science and Engineering

at the

Worcester Polytechnic Institute

May 2021

APPROVED:

_____

Diran Apelian
Professor and Provost Emeritus
Thesis Advisor

_____

Brajendra Mishra
Kenneth G. Merriam Distinguished Professor of Mechanical Engineering
Director, Department of Materials and Manufacturing Engineering

Abstract

This study investigates the relationship between mold coating wear and geometry to heat transfer coefficient (HTC) in permanent mold castings. Mold temperatures were measured using inserted thermocouples and inserted fiber optics using two different test molds. Mold temperatures were simulated by altering the heat transfer coefficient utilizing commercial solidification software. The results showed a uniform HTC was not accurate enough to simulate temperatures. Simulation of convex tooling surfaces required higher HTC as compared to concave surfaces. As mold coating wore in use, mold temperatures increased. Fiber optics were proven to be a feasible method to measure temperatures in permanent molds. In conclusion, mold coating wear and tooling geometry have major impact on HTC; changes to HTC due to air gap formation requires a multiple step heat transfer coefficient for accurate simulation. The operating HTC in permanent mold castings that were the focus of this study is a variable that changes with time from the onset of solidification, as well as with coating thickness deposited on the mold surface. Utilizing a HTC function that varies with time in the solidification software resulted in fidelity with the industrial data generated from the plant.

Acknowledgments

I am thankful for all the gifts I have been given and strive to utilize them each day to which I hope this thesis serves as an example.

I want to thank everyone who professionally and personally supported me while I studied for my degree. I am grateful to everyone at ATEK, especially Mark Osmanski who encouraged me to pursue the degree and Dan Jablonski who helped perform the trials. Also, I want to thank Linamar Corporation for the use of their test mold.

Academically, I am grateful for all the support and research guidance received from Dr. Diran Apelian, my thesis advisor. Additionally, I appreciate all the help from Rod Riek and Dr. Victor Okhuysen, FEF Professor at Cal Poly for their helpful comments on the manuscript. While working on this project, I enjoyed collaborating with Dr. Shadi Darvish and Dr. Ron O'Malley's team at Missouri University of Science and Technology, and I acknowledge their support and assistance with my work.

Table of Contents

1 Introduction

Aluminum molding materials can be divided into permanent, which can be reused, and non-permanent molds, which must be discarded each time. Non-permanent molds are the oldest form of molding material, and primarily made from heat resistant materials like silica sand and ceramic slurries [1] [2]. In non-permanent molds, the heat transfer between the casting and mold material is primarily controlled by how the slow rate of heat transfer into the insulating mold, which leads to slow solidification rates. In contrast, permanent molds are usually made from heat conductive materials like tools steels, cast iron, copper, and graphite. Due to high thermal conductivity, heat transfer in permanent molds is primarily controlled by the metal mold interface which generates faster solidification rates [3].

There are two major obstacles to using permanent molds with aluminum alloys: high solidification rates can make it difficult to fill castings before feed paths solidify and aluminum will chemically attach (solder) to ferrous materials which causes die soldering. Industrially, there are two distinct permanent mold casting methods, high pressure die casting and gravity/low pressure permanent mold casting, employed to overcome these problems. In high pressure die casting, the mold is filled as quickly as possible to ensure a complete casting, and generally die lubricants and high amounts of iron are added to prevent die soldering. Due to fast solidification rates and skin formation, high pressure die castings can have some of the best mechanical properties for aluminum castings, but they can also have high oxides and air entrapment. Not all die casting alloys can be heat treated because die lubricants and entrapped air can lead to blistering defects [2] [1].

Instead of filling the mold as fast as possible, gravity/low pressure permanent molds are covered with ceramic based coatings on casting surfaces which improve fluid flow and prevent die soldering. Since ceramics are insulators, mold coating impedes the heat transfer at the metal mold interface leading to slower solidification rates than high pressure die castings. Generally, the as cast mechanical properties of gravity/low permanent molds will be lower than high pressure die casting, but castings can contain lower amounts of iron and entrapped oxides and air. The texture of the ceramic coating helps to fill the casting but causes rougher surface finishes as compared to high pressure die castings. Additionally, gravity/low permanent mold castings will not experience blistering defects and can be easily heat treated [2] [1].

The ceramics coatings used in gravity/low permanent mold castings are critical to heat transfer across the metal mold interface and directly influences properties of the resulting casting. Unfortunately, mold coating is a complex topic with many functions still not completely understood. Commercially, there are a wide variety of coatings available but generally they can be divided into insulating coatings, texture coatings, and release coatings usually graphite based. On a single mold, multiple layers of three coating types can be manually applied; different areas of the same mold may have different coatings to promote or impede solidification. A single foundry is likely to use varied combinations of coatings across different molds to suit their needs [2]. To further complicate matters, mold coatings are impermanent and must be removed then reapplied on a regular basis due to coating wear or spalling, which is related the draw angles of the molding surface. Industrially, the coatings should be re-applied before coating related defects such as misruns, drags, and spray chips [4] start to appear which can vary mold to mold. Since mold coatings are so critical in permanent mold process, especially with regards to heat transfer, changes in heat transfer coefficient from mold coating wear is an important topic.

Effectively measuring heat transfer coefficients in castings has been a widely researched topic for decades with many different casting designs and measuring methods being used [3] [5] [6] [7] [8]. Apart from purely scientific interests, heat transfer coefficients are commercially critical inputs into the simulation modeling used to predict flow or shrinkage defects in castings. Ideally, modeling is used before permanent molds are fabricated due to high costs and long lead times associated with constructing and altering existing molds. A single mold change could easily result in tens of thousands of dollars and weeks of delays. With increasing customer demands and the nature of complex supply chains, simulating a mold and casting correctly the first time becomes a boon to all those involved [9].

2 Objectives

The two objectives of this work are: *(i)*To experimentally measure temperature differences through the casting cycle with a new and worn mold coating, and to use simulation software to recreate the experimental results using the appropriate heat transfer coefficient values; and *(ii)*To compare separate permanent mold and instrumentation methods to measure temperatures through the casting cycle with coating differences. Traditional thermocouples were used in a production environment to measure the effect on heat transfer of actual coating wear, while embedded fiber optics with a simulated worn coating was used in a laboratory setting.

3 Literature Review

3.1 Solidification Overview

The solidification of metal casting involves thermodynamics, phase transformation, transport processes, and solid mechanics. Solidification can be evaluated at the level of microscopic crystal growth, intermediate solidification front morphology, or macroscopic casting geometry through foundry process modeling, which is the focus of this paper. The main characteristics of solidification fronts were well described by Flemings in 1974 [3]; with increasing rates of solidification leading to the breakdown of the solidification front first into cellular grains followed by a dendritic structure. This breakdown of the solidification front is caused by under-cooling from solute enriched liquid at the solidification front. Once the front is disturbed, it will break down into cellular and dendritic structures. For solidification to occur, the metal's superheat and latent heat of fusion must be removed from the liquid metal through the solid metal to the metal mold interface and finally through the mold. Heat will be transferred through the mold and metal mold interface differently depending on the mold material as clearly described in Figure 1 [6].

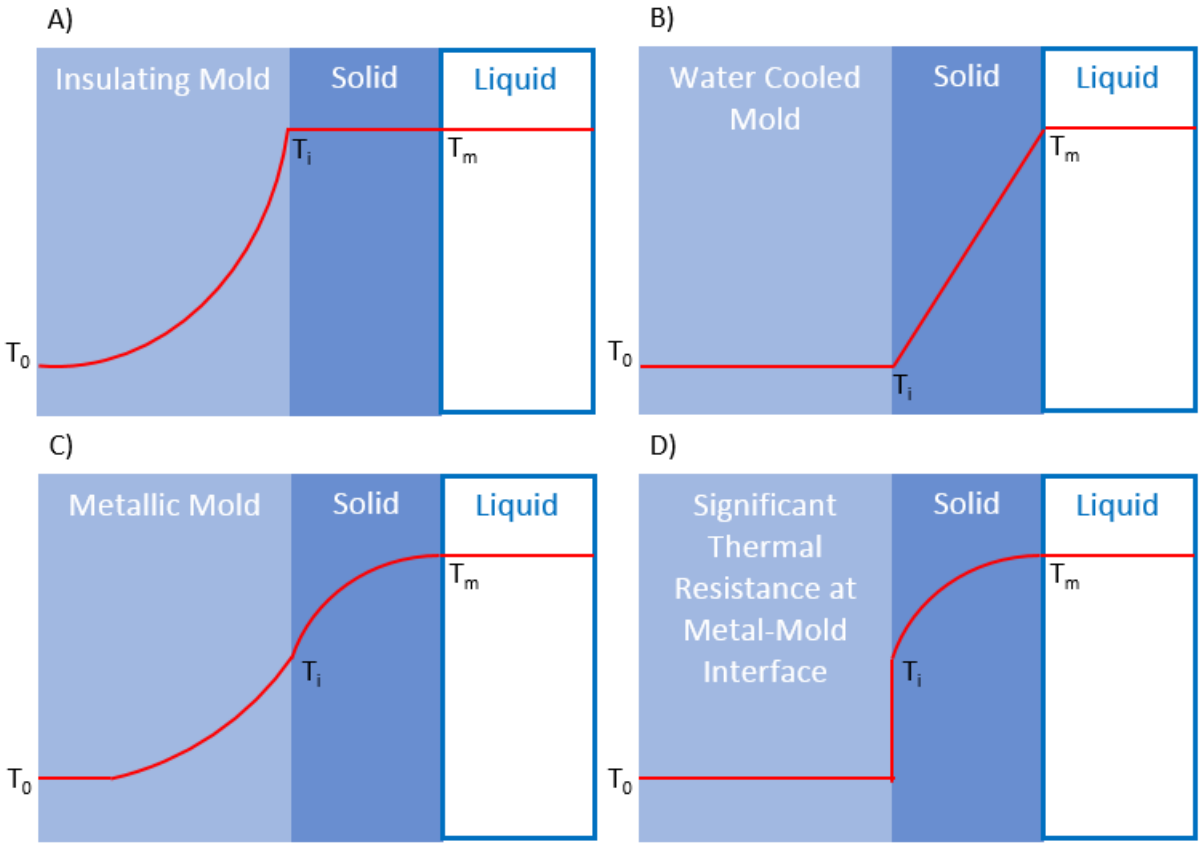

Figure 1: Heat Transfer through Various Mold Materials: (A) Insulating Mold, (B) Water Cooled Mold, (C) Metallic Mold, and (D) Significant Thermal Resistance at Metal Mold Interface [6].

As shown in Figure 1, heat flow in castings does not follow a steady state with thermal resistances caused by different mold materials critical to solidification. Heat flow in permanent mold and die casting processes are controlled by the thermal resistance at the metal mold interface as shown in Figure 2. In these cases, the solidification thickness can be defined as a function of temperature gradient, time, density, heat of fusion, and thermal resistance as defined by the variable h for heat transfer coefficient (Equation 1) [3].

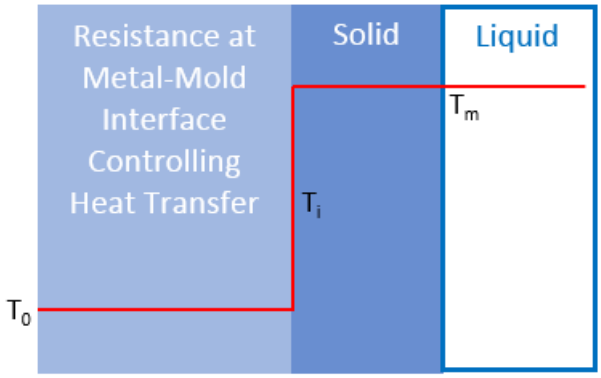

Figure 2: When Metal Mold Interface Controls Heat Transfer through Flat wall [3].

$$S = h\frac{T_m - T_0}{\rho_s H}t \tag{1}$$

S: solidification thickness,
h: heat transfer coefficient,
T_m: liquid metal temperature,
T_0: ambient temperature,
ρ_s: density of solid,
H: heat of fusion,
t: total solidification time

3.2 Heat Transfer Coefficient (HTC)

The transfer of heat across a casting and mold interface is difficult to completely breakdown into individual components because there are many mechanisms occurring simultaneously. To simplify matters one variable in simulation and modeling, heat transfer coefficient (h, HTC), is used to define heat transfer at the interface and can be used interchangeably with interface heat transfer coefficient (IHTC). This value is usually represented by h; the value of heat transfer coefficient varies widely based on process parameters. In 2004, Hines compiled heat transfer coefficient values of aluminum permanent molds measured experimentally [5]. The max values ranged from 1,500 to 20,000 $Wm^{-2}K^{-1}$ with variations in thermocouple location, mold material, alloy, and casting geometry, so just within a single casting process there exists many variations of HTC. Most experiments result in measuring a specific set of process parameters and try to determine broad relationships, but there is just so much variability inherent in the casting process [5]. Practically, a heat transfer value must be used as an input in numeric and computer modeling. It is feasible to assume a single value for heat transfer at the interface, but generally this is an oversimplification as the variable will change with time. As the casting solidifies, it will pull away from the mold surface resulting in a continually changing heat transfer coefficient. Also, changes in pressure and die temperatures fluctuate over time impacting the value [10]. Due to local metallostatic pressures and distortions caused by differences in casting geometry and liquid to solid shrinkage, a single

HTC value applied to all surfaces in the same casting would also be an oversimplification. What heat transfer coefficient value should be used in modeling becomes an overly complicated question. To further complicate matters even if the HTC is measured experimentally, small errors in temperature measurements can lead to large variations in IHTC [5].

Calculation of Heat Transfer Coefficient

There have been many formulations and expressions used to calculate heat transfer coefficient across the metal mold interface, and they can be divided into three general categories. The first group relates heat transfer coefficient (h) to changes in heat flux, and the second group relates HTC to conduction/radiation through the interface. The third group compares experimental and calculated temperatures looking for the lowest amount of error between the two values. Technically, heat transfer is not being calculated but it is iteratively assigned in modeling and compared to experimental values. The third group takes the form as shown in Equation 2 with the goal to reduce the error value as much as possible by reducing the difference between calculated and experimental temperatures [11].

$$Error = \Sigma \quad \sqrt{(T_{calculated} - T_{experimental})^2} \tag{2}$$

In the case when h is expressed as a function of heat flux (the first group), we observe higher values of h resulting in less resistance to heat flow and greater heat flux as shown in Equation 3 [5]. As can be seen in Equation 4, Equation 3 can be easily rearranged to solve for heat transfer coefficient (h). Heat flux (q) is based on the thermal gradient and thermal conductivity at the interface which is based on the change in temperature and change in distance as shown in Equation 5. Experimentally, heat flux is estimated through inverse heat transfer analysis methods as originally defined by Beck [12]. The major drawback of the Inverse method is that it is limited to one-dimensional heat transfer systems. It can be difficult to effectively apply the inverse method to castings with complex geometries [13].

$$HeatFlux(q) = \frac{h}{T_{Casting} - T_{Die}} \tag{3}$$

$$h = \frac{q}{T_{Casting} - T_{Die}} \tag{4}$$

$$q = -k\frac{\delta T}{\delta x} \tag{5}$$

The second main group of formulations base heat transfer coefficient (h) on the conductivity at the interface. As a more complex example, heat transfer can be assumed as the sum of metal-to-mold conduction (h_{mc}), conduction through the air gap (h_{gc}), and radiation through the air gap (h_{gr}) as reflected in Equation 6 [10]. Since heat transfer through radiation is minimal in aluminum alloys, it is usually omitted. In practice, the conduction through the air gap becomes the driving force for heat transfer, so there are equations estimating heat transfer coefficient based solely on the air gap such as Equation 7. Due to their simplicity, these estimations require accurate measurements of the air gap conductivity and distance [14].

$$h = h_{mc} + h_{gc} + h_{gr} \tag{6}$$

$$h = \frac{\text{Air Gap Conductivity}}{\text{Air Gap Width}} \tag{7}$$

There exists a fourth group of equations that relate heat transfer coefficient to process parameters such as time, pressure, and temperature. Such quantitative expressions are experimentally derived and represent the specific process being measured; they show functional relationships between variables but do not have broad applications. As an example, Natsume et al. derived a relationship between solidification time (t) and heat transfer coefficient (h) clearly described in Equation 8. Two constants (a,b) had to be experimentally derived resulting in the updated formula of Equation 9 [15]. Ilkhchy, Jabbari, and Davami derived a nonlinear relationship between applied pressure (P) and heat transfer coefficient (h) (Equation 10) [16].

$$h = at^{-b} \tag{8}$$

$$h = 9735.5t^{-0.377} \tag{9}$$

$$h = 0.0011P^3 - 0.112P^2 + 6.605P + 2924.57 \tag{10}$$

Measurement of HTC

As implied in the previous section, there are two distinct ways to measure heat transfer coefficient (h, HTC) at a metal mold interface. The first method is measuring the size of the air gap formed, and estimate HTC based on this value. The second method is to measure temperatures in the mold and metal to deduce HTC through the inverse method [14]. In addition to the second method, simulation software can be used to reproduce the recorded temperatures through the iterative adjustments of heat transfer coefficient in simulation software [17]. A variety of measurement devices have been used for these methods.

Measurement of Air Gap

To measure the air gap, displacement gauges are used to measure the movement of the casting and mold. It is possible for permanent molds to move relative to the casting surface during solidification but it so much more likely for non-permanent molds, especially silica sand molds, to move during solidification. Once the distance of the air gap is known, a relatively simple formula, h=k/x, can be used to estimate the heat transfer coefficient, h, with k equal to the thermal conductivity of the air-gas mixture and x equal to the distance of the air gap. In 2005, Kulkarni and Radhakrishna used this method to estimate the heat transfer of aluminum in CO_2 sand molds and found the estimated value very dependent on the assumed thermal conductivity of the air-gas mixture. As compared to inverse measurements taken in the same trial, the air gap HTC values were found to be ten times lower [14].

Kulkarni and Radhakrishna used ceramic tubes embedded in the mold to measure displacement [14], but there are other methods available. Fiber optic fibers can be used to measure spatial as well as temperatures within a single mold as shown by Roman et al. making it feasible to calculate HTC using the air gap and inverse method simultaneously [18]. Additionally, ultrasonic probes can be used to measure gap formation. The ultrasonic signal will reflect uniquely off materials with

different density, so the aluminum casting will reflect differently from the mold. As the aluminum casting surface moves away from the mold, the delay of the reflected signal will increase, thus measuring the air gap [19]. The ultrasound method was used by Weng et al. to measure air gap in the thixocasting process and calculate the heat transfer coefficient. The process requires an accurate estimate of air gap conductivity, but it can be used in situations with non-1-D heat transfer. The round-trip delay (t_d) can be correlated to heat flux (q) which relates by to heat transfer coefficient [13].

Measurement of Temperature

The most common method to measure temperature in casting trials utilizes the insertion of thermocouples in the mold and casting [14]. It is relatively easy to drill a hole in a metal mold to place a thermocouple for measurement. Understandably over the decades, the many studies have used thermocouples to measure temperatures, but there are downsides. Once a thermocouple is used in a casting it cannot be reused, so it can be difficult to run repeatable studies with many iterations [17]. Functionally, there can be areas in the mold where it is impossible to place a thermocouple which is often the area of interest. Since thermocouples only represent one measurement point, it would be ideal to place many thermocouples, but too many thermocouples start to alter the thermal properties of the mold [18]. Additionally, the increased amount of cabling required for large numbers of thermocouples can easily lead to complexity and inaccurate measurements [20]. Ideally, a thermocouple would be placed in the mold as close to the casting surface as possible, but over time this will cause the mold to crack reducing reproducibility of trials. Since thermocouples must be placed a safe distance from the casting interface, there are delays in temperature readings. To overcome these problems inherent with thermocouples, a variety of other measurement devices have been used.

To solve the reproducibility problem, Dour et al. used a sapphire light pipe connected with a monochromatic pyrometer to measure temperature in high pressure die castings. When the die was opened, the pyrometer was impacted by surrounding light sources, so readings could only be taken with a closed mold. The pyrometer had to be calibrated for the emissivity of each alloy used, but gauge was found to be reasonably accurate. For measuring heat flux density, the estimated uncertainty was between 3% to 35% for the heat transfer coefficient [17].

With the development of fiber optic interferometer sensors, the problems associated with using multiple thermocouples could be eliminated. Multiple temperature measurements can be taken along the same fiber up to 50 meters in length with temperature measurements taken at 0.65 mm intervals [18] with an example of a fiber optic shown in Figure 3. This measurement technique is primarily limited by the degradation of Rayleigh back scattering signals which are impacted by elevated temperatures ($> 500°C$). Higher temperatures lead to bleaching of optical fibers, and the complete erasure of the sensors at $> 700°C$ [21].

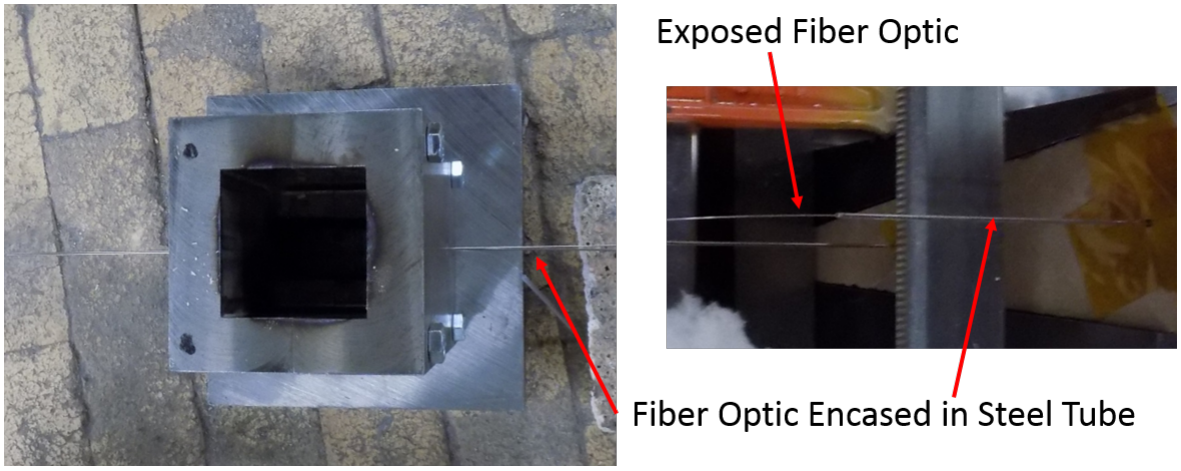

Figure 3: Example of exposed and steel encased fiber optic from recent trials.

Recent work has been performed to increase the temperature range. In 2020, Roman et al. used an optical frequency domain reflectometry (OFDR) interrogator system on an unmodified optical fiber to prevent temperature decay, and with the use of a steel tube could accurately measure temperatures exceeding $> 700°C$, which could lead to future use by metal casters. These measurements were found comparable to standard thermocouples, but the fibers did require continuous thermal contact for reliable measurements [18].

In addition to elevated temperatures, fiber optics can also be impacted by electromagnetic stirrers which are commonly used in ferrous castings and forging processes. In research aimed at the forging industry, Lieftucht et al. used Fiber Briggs Grating (FBG) to eliminate the electromagnetic problems. FBG separates the fiber optic into individual gratings spaced at set intervals which reflect their own individual wavelength and temperature measurements. This grating method is insensitive to electromagnetic fields and will change proportionally under thermal and mechanical expansion [20].

Influences on HTC

After reviewing numerous studies measuring heat transfer coefficients under many different process parameters, a multitude of variables can impact HTC. Additionally, the specific HTC values seem to relate directly to the exact process parameters, but there are general relationships between parameters and heat transfer coefficients. The process parameters with the strongest impact on heat transfer, in no order are pressure, part geometry, mold materials, mold thickness, alloy composition, mold temperature, and metal temperature. The impact of each variable will vary based on the time of the solidification cycle [22].

In general, the evolution of the heat transfer coefficient can be divided into three stages based on increasing solidification time. During the first stage, the metal is liquid with the highest heat transfer values reached, and the following process parameters have the greatest influence metal temperature, mold surface roughness, and mold temperature having the greatest impact. As the liquidus temperature is reached and thin shell starts to form on the castings surface leading to the second stage. The shell slows down heat transfer but applied pressure can be used to maintain constant contact between casting and mold. During the third and final stage, the casting's skin is able

to resist metallostatic pressure, which generally occurs between liquidus and solidus temperatures. At this stage, the casting pulls away from the mold wall creating an air gap, heat transfer reaches its lowest values, and all parameters relating to air gap formation have the strongest effect [22].

Metal Composition and Temperature

In general, lower surface tension will improve the fluidity of liquid aluminum, which will increase the amount of heat transfer at the metal mold surface. At a higher temperature of the alloy's liquidus temperature (superheat), the molten aluminum can interact with more of the mold surface. The formation of a thick rigid shell on the metal surface will reduces heat transfer with the mold, but increased superheat will slow the formation of a thick shell leading to more heat transfer. Studies performed with aluminum alloys have shown 115°K superheat had three times the heat transfer of the similar alloy with 40°K superheat [23]. In a 2005 study, Ferreira et al. looked at the effect of superheat in Al-10wt%Cu and Al-4.5wt%Cu alloys. They found a similar relationship between HTC and superheat, but also discovered the sensitivity of superheat's influence is relative to the thermal conductivity of the mold. Superheat will have a larger effect on HTC with higher thermal conductivity molds [24].

As a comparison to superheat, which is the temperature above liquidus, semisolid casting processes are concerned with the initial solid fraction of the alloy. Kuo et al. looked at the impact of solid fraction on magnesium alloys (AZ91D) in steel molds and compared the heat transfer coefficient to a liquid based casting process using SKD-61. The liquid and semisolid heat transfer coefficient (h, HTC) values as defined by a h-T graph (Figure 4) followed different evolution patterns. The liquid based h-T graph can be distinguished by five stages. Stage 1 showed a sharp decrease in HTC as a shell begins to form. Stage 2 had a secondary peak value which was slowly reached as pressure pushes against the shell. Followed by a solid skin starting to form in the third stage. Next, hydrostatic pressure continues to push the solid shell against the mold. In the fifth stage, the shell was strong enough to resist the pressure; the casting begins to shrink leading to an air gap [25].

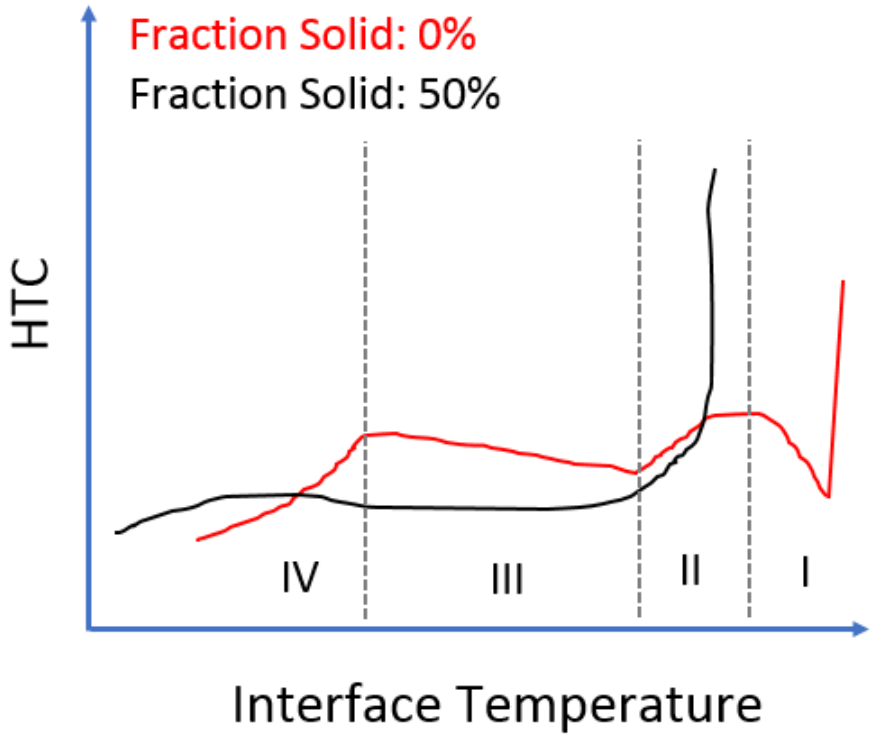

Figure 4: Heat Transfer Coefficient v. Interface Temperature based on Fraction Solid [25].

For the semisolid casting process, Kuo et al. found the HTC followed a different pattern with the first stage immediately followed by an exceptionally long and gradual fifth stage. Higher solid fractions showed a steeper drop in the first stage, but both solid fractions measured had relatively the same values in the fifth stage showing a more uniform solidification as compared to the liquid casting solidification [25].

In addition to superheat, an alloy's surface tension can be impacted by alloying elements. By lowering the surface tension, the alloy will make better contact at the mold interface leading to higher initial IHTC values. As for specific examples, increasing magnesium content in Al-Mg alloys lead to lower surface tensions, silicon reduces tension in Al-Si alloys, but not all elements have an impact for instance varying copper in Al-Cu alloys has no effect on surface tension [26]. With regards to the effect of Si in Al-Si, Taha et al. found that once superheat dissipated the Al-Si alloy had the same heat transfer coefficient as pure aluminum. It was the existence of a mushy zone which created the difference in heat transfer, and without the mushy zone (no superheat) there was no difference as compared to pure aluminum. The impact of alloying elements on heat transfer is interrelated to the amount of superheat [22].

While this work is focused on heat transfer in aluminum permanent molds, different primary alloys will impact heat transfer coefficient due to intrinsic properties such as latent heat. As compared to aluminum alloys, magnesium alloys have a smaller volumetric latent heat, which leads to a lower total heat flux and a faster cooling casting. Despite differences in latent heat, Dargush et al. found interface characteristics such as surface roughness to have a stronger impact on heat transfer coefficients after studying Al-9Si-3Cu and Mg-9Al-1Zn die castings [27].

Mold Roughness, Material, and Coating

The interfacial heat transfer coefficient (IHTC) is also impacted by the type of mold coating, type of mold material used, and the surface roughness of the interface. Functionally as liquid metal is poured into the mold, air inside the mold cavity is displaced and exits through mold venting, but some air will become trapped within the troughs on the molding surface. These pockets of air lead to imperfect contact between mold and casting that can be described as point contact. Heat travels from the casting to the mold more efficiently through these contact points vs. the air gaps as shown in Figure 5 [22]. In a 1997 study, Assar showed IHTC decreases as surface roughness increases using zinc cast in steel molds. The rougher surface is unable to come into full contact with the metal interface because of trapped air pockets between the liquid metal and mold interface. Since stagnant air behaves as an insulator, the IHTC value decreases [28].

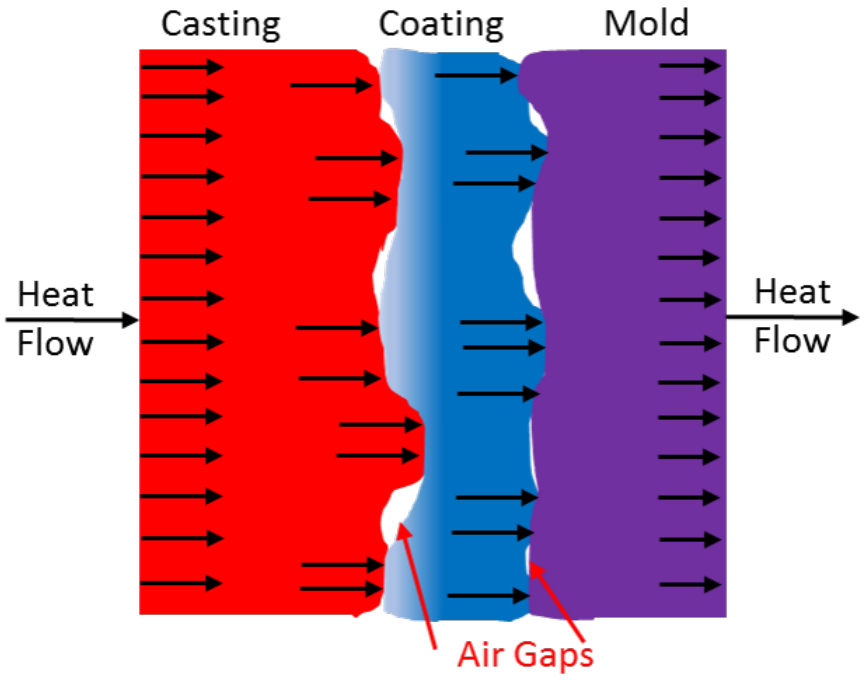

Figure 5: Heat flow from casting to mold through mold coating by point contact around air gaps [22].

A perfectly smooth polished mold surface would be ideal, but mold coating is required in aluminum permanent castings to allow the casting to fill before solidification occurs and to prevent aluminum from chemically attaching to ferrous molds, [26] but there are specific molding materials which do not require a mold coating such as graphite [29]. In terms of mold coatings, the release coating is primarily made from graphite, so it is logical for graphite molds to not need mold coating. Bazhenov et al. compared the IHTC values between A356 aluminum ingots cast in steel molds and graphite molds and found peak IHTC values for graphite molds to be 2-3 times higher than the steel molds. The steel molds ranged from 1300-3000 $Wm^{-2}K^{-1}$ while the graphite molds ranged from 1800-4700 $Wm^{-2}K^{-1}$[11]. Prabhu and Suresha combined graphite mold inserts and superheat to achieve increases in heat flux ranging from 5-25% but found superheat to have higher significance on heat flux [30]. Graphite molds could solve the coating problem, but it would not

solve the filling problem. Graphite mold inserts could be used as chills in thin to thick sections away from feed paths, especially in the top die (cope), to promote directional solidification.

When mold coatings are required for castings, coatings will affect the IHTC because mold coating exists to lower the thermal conductivity of the mold. Aside from surface roughness, conductivity of mold coating is controlled by composition, porosity level, thickness, and microstructure. In general, mold coatings range from 50-200 microns [31]. In 2007, Hamasaiid et al. specifically measured the impact of coating material and thickness on IHTC. There was only a weak difference found between a ceramic (TiO_2) and graphite coating. The thermal conductivity for TiO_2 coating was 0.45 $Wm^{-2}K^{-1}$ and 0.60 $Wm^{-2}K^{-1}$ for graphite coating. Increased coating thickness was found to significantly increase solidification time for Al-9Si-3Cu and Al-7Si-0.3Mg alloys. As layers of coating are applied air pockets will become trapped in the coating leading to lower thermal conductivity, so increased thickness equates to more trapped air pockets [26]. Coates and Argyropoulos found surface roughness impacted the formation of air gap at the metal mold interface. With lower surface roughness leading to earlier formation of an air gap, but once the gap forms the surface roughness becomes less important. Furthermore, they found the amount of superheat was a greater factor on heat transfer coefficient than surface roughness [23].

Rough or porous surface coatings do not only have to be created through mold coating. Schmidt used a stainless-steel plasma spray to apply a rough surface to a steel mold, which created a surface roughness of 22 μm. Then compared this surface to a smooth uncoated die and a coated mold, which was 240 μm thick with 50% porosity. Through this experiment, Schmidt confirmed trapped air impacted heat transfer. Heat transfer coefficient on the smooth dies ranged from 20,000 to 30,000 $Wm^{-2}K^{-1}$, while the plasma sprayed surface had a value of 2,000 $Wm^{-2}K^{-1}$. The mold coating surface measured 700 $Wm^{-2}K^{-1}$; with just an increase in surface roughness of the mold from polished steel to 22 μm (plasm sprayed), the heat transfer coefficient dropped dramatically which proves the impact of trapped air on the heat transfer coefficient [32].

Pressure and Part Geometry

While the solidification fraction of a casting is low (less than 30% depending on the alloy), added pressure can be used to maintain close contact between the aluminum casting surface and the mold wall. As the solid fraction increases, the pressure transfer paths close, and pressure's impact on heat transfer is reduced. In die castings, which use no mold coatings and use high pressures, heat transfer coefficients can average 19,000 $Wm^{-2}K^{-1}$ with values reaching 80,000 $Wm^{-2}K^{-1}$. Since much higher pressures are used in die castings, pressure has an over-sized impact on heat transfer, but pressure still affects heat transfer in permanent mold and low-pressure permanent mold castings. In terms of die castings, Guo et al. found pressure had a greater influence at smaller casting thicknesses with changes in process parameters only affecting the peak HTC value but not the overall HTC curve [33].

In a 2012 study Ilkhchy, Jabbari, and Davami specifically measured the effect of pressure on aluminum permanent mold castings using A356 and externally applied weight, up to 300 kgs, to vary the amount of applied pressure, which reached up to 1.66 MPa (244 psi). In trials with no extra applied pressure, they found the Equation 11 could be used to calculate the heat transfer coefficient (h) using only the solidification time (t) as a variable. When extra pressure was applied, they found heat transfer could be correlated to pressure (P) using Equation 12, which shows the relationship between pressure and HTC is not linear and increases with more applied pressure [16].

$$h = 4559t^{-0.44} \tag{11}$$

$$h = 0.0011P^3 - 0.112P^2 + 6.605P + 2924.57 \tag{12}$$

As a comparison, Aweda and Adeyemi performed similar pressure/HTC based experiments but using aluminum (commercially pure) squeeze castings. As with the previously mentioned study, Aweda and Adeyemi found a polynomial relationship between heat transfer coefficient (h) and pressure (P), but they also found variations in the formula based on metal temperature (T), which will be discussed further in this paper. When temperatures were below solidus ($< 500°$C), Equation 13 could be used, and above the liquid phase ($> 660°$C) Equation 14 was more accurate. Between liquidus and solidus ($500 - 660°$C), Equation 15 should be used [34]. There was not complete agreement between the two studies, but it is obvious from all the derived formulas that higher pressure results in higher heat transfer coefficients. The two groups were measuring different metal casting processing and alloys, so some difference in results should be expected, but in reviewing multiple studies it is obvious HTC is exceedingly difficult to consistently measure due to all the impacting values.

$$h_S = 3.081T + 1.303P - 232.942 \tag{13}$$

$$h_L = 2.769T + 2.518P + 988.92 \tag{14}$$

$$h_{LS} = 10.420T + 5.641P - 4176.022 \tag{15}$$

Pressure applied at the mold metal interface is not limited to externally applied pressure used in die castings but is also influenced by the position within a casting. Lin, Zhao, and Huang used the inverse method to estimate the heat transfer coefficients for bottom and lateral surfaces in a casting. The bottom surfaces were found to have a value of 750 $\mathrm{Wm^{-2}K^{-1}}$ which was three times greater than the lateral surface. In addition to the differences in HTC, the bottom surface HTC took longer to stabilize showing fluctuations in peak HTC value. Lin, Zhao, and Huang theorized these fluctuations were caused by hydrostatic pressure from the liquid metal pushing against a thin solidifying shell. The bottom max HTC only stabilized once the shell was thick enough to resist the pressure. This fluctuation also created many convex surfaces with small height differences on the bottom of the casting. In comparison, the lateral casting surface had a single large convex surface with a large height difference [35]. In agreement with Lin and team, Taha et al. found the casting's bottom surface to have four times the heat transfer value as the top surface and twice the value as the lateral or side surfaces. They found the differences in heat transfer by casting position accentuated by higher amounts of superheat [22] Instead of many small convex surfaces, Griffiths observed the formation of a large convex casting bottom surface in a highly cooled chill mold [7]. It is likely the highly cooled mold surface created a casting shell thick enough to resist the hydrostatic pressure, which lead to shorter contact with the mold wall thus no small convex surfaces. The formation of large enough convex surface would lift the periphery edges of the casting away from the chilled surface forcing the casting's center to be preferentially heated [36]. As the casting solidifies, the interaction between neighboring geometries will impact heat transfer by increasing or decreasing contact with the mold surface.

Not only position within a casting impacts applied pressure, but overall casting height relates to the total hydrostatic pressure in a casting with a greater height resulting in a higher hydrostatic pressure. Akar et al. studied the impact of casting height in Al-Si 12.9% alloy using casting heights of 100, 150, and 200 mm. They measured higher peak HTC values and a delay in air gap formation with higher casting heights due to the extra hydrostatic pressure pushing against a thin solidifying shell [37]. A bottom surface in a tall casting should experience a maximum amount hydrostatic pressure and have the highest HTC value.

Aside from position within a casting and casting height, the shape of individual geometric features will affect heat transfer. In a 2012 study, Bertelli et al. looked at differences in HTC in hollow cylindrical castings due to concave (inward solidification) and convex mold surfaces (outward solidification). They found a relationship based on geometric differences shown in Equation 16. With constant a relating to the alloy, and constant m to the mold. Solidification time is t, and h is of course heat transfer coefficient. During inward solidification (concave surface), the Equation 17 should be used, but with outward solidification (convex surface) the Equation 18 is used. Bertelli et al. were able to prove this relationship with experimental trials using aluminum and lead based alloys. Based on this equation, a convex mold surface at the metal mold interface will have a higher heat transfer coefficient. As the casting solidifies, it shrinks and wraps around the convex mold surface maintaining contact for longer. In contrast, the casting will shrink and pull away from the concave mold surface during solidification leading to a lower HTC [38]. In agreement with Bertilli et al., Chen and Im showed heat will extract from a convex corner at a higher rate than a concave corner.

$$h_{metal/mold} = at^{+/-m} \tag{16}$$

$$h_{metal/mold} = at^{-m} \tag{17}$$

$$h_{metal/mold} = at^{m} \tag{18}$$

While Bertelli et al. focused only on concave and convex surfaces using cylinders [38], there are many other casting shapes. When performing a heat transfer study comparing graphite molds and boron nitride coating, Sabau compiled heat transfer coefficient values for common geometric features. Values for plates ranges from 200-700 $Wm^{-2}K^{-1}$, and tubes were 3000 $Wm^{-2}K^{-1}$. Measurements for cylinders ranged from 2000-3000 $Wm^{-2}K^{-1}$ [12].

As an extension of geometry, thickness of a casting will impact the heat transfer coefficient, but not the peak HTC value. Hamasaiid, Dargusch, and Dour measured HTC in castings with thicknesses of 15 mm, 20 mm, and 25 mm. During HTC evolution over a casting cycle, they saw a second plateau in HTC relating to the formation of the eutectic phase. Casting thickness impacted the length of this plateau with increased thickness leading to a longer plateau [31].

Air Gap Formation

In addition to the pockets of air trapped at the metal mold interface due to surface roughness, the formation of a complete air gap between the casting and mold plays a critical role in heat transfer in aluminum permanent molds. As a casting solidifies, the metal front pulls away from the metal mold interface creating an air gap which widens with further solidification. Before the air gap is

formed, heat is primarily transferred from the casting to the mold wall through conduction, but as the air gap forms conduction is greatly hindered as stagnant air is an insulator. Convection had a negligible effect at the air gap, and an insignificant amount of heat will be transfer by radiation from the casting surface in typical aluminum alloy casting temperatures. Physically, the air gap will form due to inhomogeneous cooling and casting shrinkage leading to stresses and distortions creating the air gap [39].

The development of the air gap can be described based on changes in rheological behavior of the casting during solidification. As soon as the liquid aluminum starts to solidify but before the coherency point, it will behave like a liquid but not completely as a liquid because dendrites are starting to grow within the liquid. As the coherency temperature is reached, a solid skeleton of dendrites begins to build up at the casting surface. At this point the surface starts to behave more like a solid with pseudoplastic behavior. Further in solidification, the casting will pull away from the mold surface forming the air gap [40]. The air gap formation requires the density of the solid is greater than the density of the liquid ($p_s > p_l$), which is the case in most metals, and causes the metal ti shrink during solidification [6].

Specifically, it is the air gap's thickness affecting the heat transfer, but thickness will vary throughout solidification. Ahmadien et al. measured the impact of air gap using quartz rods attached to a linear variable differential transformer (LVDT) and thermocouples in an A356 permanent mold, but the mold's coating condition is unclear. They found gap growth slowly increased from 0-80 seconds; the casting surface temperature at 80 seconds was close to solidus. The maximum amount of gap growth rate occurred from 80 to 200 seconds, slowed after 200 seconds, and completely stopped at 600 seconds. As shown in previous examples, it can be useful to divide the transformation of heat transfer coefficient into two stages and divide a relationship for each stage. Based on these results, Ahmadien et al. suggested using an HTC of 5000 $Wm^{-2}K^{-1}$ for interface temperatures above liquidus, and 350 $Wm^{-2}K^{-1}$ for below solidus. For temperatures between liquidus and solidus, the Equation 19 could be used with T representing temperature. In terms of direct comparisons between gap width and HTC, at a gap width of 0.01 mm the heat transfer coefficient was 4500 $Wm^{-2}K^{-1}$, roughly 1000 $Wm^{-2}K^{-1}$ at 0.05 mm, 500 $Wm^{-2}K^{-1}$ at a width of 0.1 mm, and 250 $Wm^{-2}K^{-1}$ at 0.2 mm. The initial air gap causes the largest changes in HTC, but the impact on HTC is reduced as the gap grows further [41].

$$HTC = -0.727T^2 + 901.2T - 274314 \tag{19}$$

Metal temperatures at the mold surface temperatures can impact the formation of the air gap leading to changes in HTC. Bazhenov et al. found decreasing mold surface contact temperatures leading to lower HTC values. At lower mold contact temperatures, the metal surface starts to contract earlier forming an air gap. When the metal contacting the mold surface had a temperature of 1000°C, the HTC was 1100 $Wm^{-2}K^{-1}$; HTC dropped to 100 $Wm^{-2}K^{-1}$ when the metal temperature at the mold surface reached 190°C [29]. In a study using cooled permanent molds Zeng, Yao, and Wang found purposely lower mold temperatures through cooling could be used to speed air gap formation. They specifically designed a mold with a moveable wall, so they could precisely control the air gap width and duration of air gap formation during experiments. The researchers measured an IHTC value of 1350 $Wm^{-2}K^{-1}$ before an air gap started to form. At a 6 mm air gap, IHTC values ranged from 75-220 $Wm^{-2}K^{-1}$ with the smaller value experiencing 140 seconds of cooling and the higher value experiencing up to 1190 seconds of cooling. With the same amount

of cooling, the IHTC values reduced to 55-155 $Wm^{-2}K^{-1}$ with an air gap of 30 mm. With greater amounts of cooling time, the variation in IHTC values from air gap reduced. At max cooling, the 6 mm air gap had a 75 $Wm^{-2}K^{-1}$ while the 30 mm air gap showed a 55 $Wm^{-2}K^{-1}$. In comparison with the lowest amount of cooling, the 6 mm gap showed 220 $Wm^{-2}K^{-1}$ and 30 mm measured 155 $Wm^{-2}K^{-1}$ [42].

The large impact of any amount of air gap at the metal mold interface is due to the low thermal conductivity of air, but it is possible to increase the conductivity of the air gap by using a different gas. Helium, which has one of the highest thermal conductivity of a gas, is non-toxic, widely available, and nonflammable, and recently recyclable due to equipment that gas suppliers have developed. As shown in a 2008 study, Argyropoulos and Carletti were able to increase heat transfer in permanent molds by using helium gas. They used a unique casting apparatus which would blow gas onto the metal mold interface. Castings made with helium had an average HTC value 48% higher than a casting made without helium. The onset of the air gap formation was also reduced by 34% with the use of helium. With A356 alloy poured into copper molds having a roughness of 0.23 microns, the average HTC was 1313 $Wm^{-2}K^{-1}$ with normal air and 1629 $Wm^{-2}K^{-1}$ with helium injection. The active insertion of normal air at the interface developed an air gap at 245 seconds, while helium caused the gap to form at 223 seconds. Helium gas was a more effective chill than normal air. As mold surface roughness increased, the differences in IHTC between air and helium became greater. With a 40.09 μm surface roughness, the air IHTC was 690 $Wm^{-2}K^{-1}$ and 1127 $Wm^{-2}K^{-1}$ for helium [43]. The heat transfer across an air gap will also change based on the mold material. The HTC of an air gap between a casting and a graphite mold is roughly 12 $Wm^{-2}K^{-1}$ [29], while the air gap between an H13 steel mold and casting is approximately 8.5 $Wm^{-2}K^{-1}$ [44]. As an aside, one of mold coating's primary purpose is to reduce thermal conductivity to aid filling, so at some point increasing thermal conductivity will start to negatively impact filling.

3.3 Solidification Modeling

Numerical Methods

Geometry based models for predicting solidification are some of the oldest and easiest to implement. These methods are based on Chvorinov's fundamental Section Modulus (SM) rule as shown in Equation 20 [45]. In applications of Chvorinov's rule, complex casting geometry can be broken into simple shapes with known V/A ratios, and the solidification time can be calculated. In general, casting areas with the same V/A ratios will solidify in the same amount of time, SM=V/A. Furthermore in 2-D casting sections, the section modulus can be reduced to casting area (A) and perimeter (P) ratios as stated in Equation 21 [45]. Once solidification times for casting sections are known, the casting can be overlaid with isotherms like a contour map used to show elevation. With isotherms in place, predictions can be made on which casting area will solidify first and on feeding distance. Ideally, all gating areas will solidify last with no isolated shrinkage areas in the casting [45].

$$t = k * (V/A)^2 \tag{20}$$

t: total solidification time,
v: casting volume,

A: casting cooling surface,
K: constant depending on physical and thermal properties of mold, alloy, and casting conditions

$$SM = V/A = A/P \tag{21}$$

Aside from predicting isotherms using casting geometry (Chvorinov's Rule), shrinkage can be predicted using Niyama Criterion, which is based on thermal gradients (G) and cooling rates (T), as described in Equation 22 [45]. This parameter can also be used with R representing solidification time (Equation 23). The use of this criterion or value is based on two observations: porosity tends to form at the last areas to solidify; and as thermal gradient decreases, porosity increases. These observations equate to $\frac{\mathrm{G}}{\sqrt{R}}$, so a low thermal gradient and a high solidification time will result in a small value, which will predict a shrinkage area. In practice, $\frac{\mathrm{G}}{\sqrt{R}}$ can be calculated at casting sections to predict shrinkage [8].

$$\text{Niyama Criterion} = \frac{G}{\sqrt{-T}} \tag{22}$$

$$\text{Niyama Criterion} = \frac{G}{\sqrt{R}} \tag{23}$$

Computational Methods

Aside from numerical models based on Chirnov's Rule or the Niyama Criteria, computational solidification modelling can be used. In general, the differences in computational methods comes down to how volume of the simulation is defined with a mesh being created for finite difference and finite element methods [46], while each element is treated like a particle in the Smooth Particle Hydrodynamics (SPH) process [47]. All the methods have their own strengths and weaknesses usually relating to accuracy and computation time.

Finite element and finite difference methods both create rectangular meshes or three-dimensional blocks. The meshes or grid can be created in a structured (finite difference) or an unstructured (finite element) fashion. With finite difference, curved boundaries are approximated through a stair step pattern while with finite element the mesh is made to conform to the casting geometry which makes the process longer and computationally taxing. [9]. These artificial staircases along curved and sloping boundaries in the finite difference method can lead to artificial diffusion and mass conservation problems [47]. In general, finite difference models tend to adopt simplified geometries and boundary conditions, but finite element models usually have more complex geometries and boundary conditions with higher computational requirements [46].

SPH method is unique from the finite element and finite difference methods because the model is not broken into a mesh but defined in terms of a disordered group of points with center of each point is interpreted as a particle. As compared to the mesh methods, this will create a more accurate flow but at higher computational cost. Due to the Langrangian nature of the SPH method, the particles will have complex flows. The smoothed approximations of the particles are used to find

the gradients of fluid flows which can be built from the Navier-Stokes equations [47] as shown in Equation 24 [48].

$$\frac{\delta U_i}{\delta t} + U_j \frac{\delta Ui}{\delta xj} = -\frac{\delta P}{\delta \rho_1 \delta x} + \frac{\delta}{\delta x_j}(\upsilon_e(\frac{\delta U_i}{\delta x_j} + \frac{\delta U_j}{\delta x_i})) + g_i \tag{24}$$

Due to differences between computational methods, it is possible to achieve slight differences in simulations using different methods. Ha et. al compared the simulations of the same aluminum casting using SPH (smoothed particle hydrodynamics) and MAGMAsoft (finite difference). Both methods were able to predict the overall structure of the filling process, but SPH was better able to predict the fine details of the flow and free surface wave behavior. In comparison, MAGMAsoft was able to predict the fluid height more accurately in the sprue [47].

With all computational models, there is a constant battle between the possible accuracy of the solidification model and the required computational time. A prevalent example is the mesh size used to define the casting and mold within the solidification model. A finer mesh size will produce more accurate simulations but will require a longer computation time than a coarser mesh. When multiple simulations are run during the development of a casting, the computation time required will be significant. For example, Zhang, Maijer, and Cockcroft found a difference between simulation and production temperatures while modeling a low-pressure wheel casting, were caused by the coarseness of the mesh used for the mold [46].

There are several commercially available software packages capable of computer simulations including ABAQUS, MAGMAsoft, EKK CapCast, and SolidCast [46] to just name a few examples, but it possible for individual researchers to create their own models. For example, Chan developed a finite element mesh to model aluminum brake drums. In general, the models need to be able to incorporate latent heat release, phase changes, temperature variant material properties, modes of heat transfer, complex heat transfer, and of course heat transfer coefficient. Additionally, the cyclic nature of the casting process including mold opening and closing must be considered [49].

4 Experimental Methods

4.1 Measurement of HTC

From the literature review, it is obvious that heat transfer coefficient is critical to accurate simulation modeling of aluminum permanent molds. Unfortunately, heat transfer coefficient is impacted by many factors including pressure, part geometry, metal composition, mold coating, and molding materials to name a few. Throughout the trials, efforts were made to maintain keep these parameters consistent or to specifically measure changes in these values such as mold coating wear and part geometry. Additionally, to measure temperature more accurately and therefore heat transfer care was taken to maximize the number of thermocouples used in the mold design.

Maximized Temperature Measurements

During the experiments two unique test molds, designated as the Linamar mold and Wedge/ACRC mold, were used to measure temperatures. The designs of both molds were altered to maximize the amount of temperature readings, and one mold was changed to additionally test the influence

of tool geometry. The Linamar mold was designed to use inserted traditional thermocouple, while the Wedge mold was designed and manufactured for inserted fiber optics.

Linamar Mold with Thermocouples

The mold used for production trials performed at ATEK was lent from the Linamar Corporation. The tool in the original state had nine thermocouples on a flat geometry side (Figure 6), and a single thermocouple on the opposite surface which contains the more complex casting geometry (Figure 7). Both sides of the mold contain casting surfaces as shown in Figures 6-7. The overall size of the Linamar mold was 250 mm wide by 200 mm tall by 200 mm thick (9.84" x 7.87" x 7.87") with each mold half being 100 mm (3.94") thick. In the center of the complex geometry mold side, there is a removable tooling insert as shown in Figure 8. The overall envelope of this insert was used as the dimensional window to create a new insert with more geometric features and thermocouples.

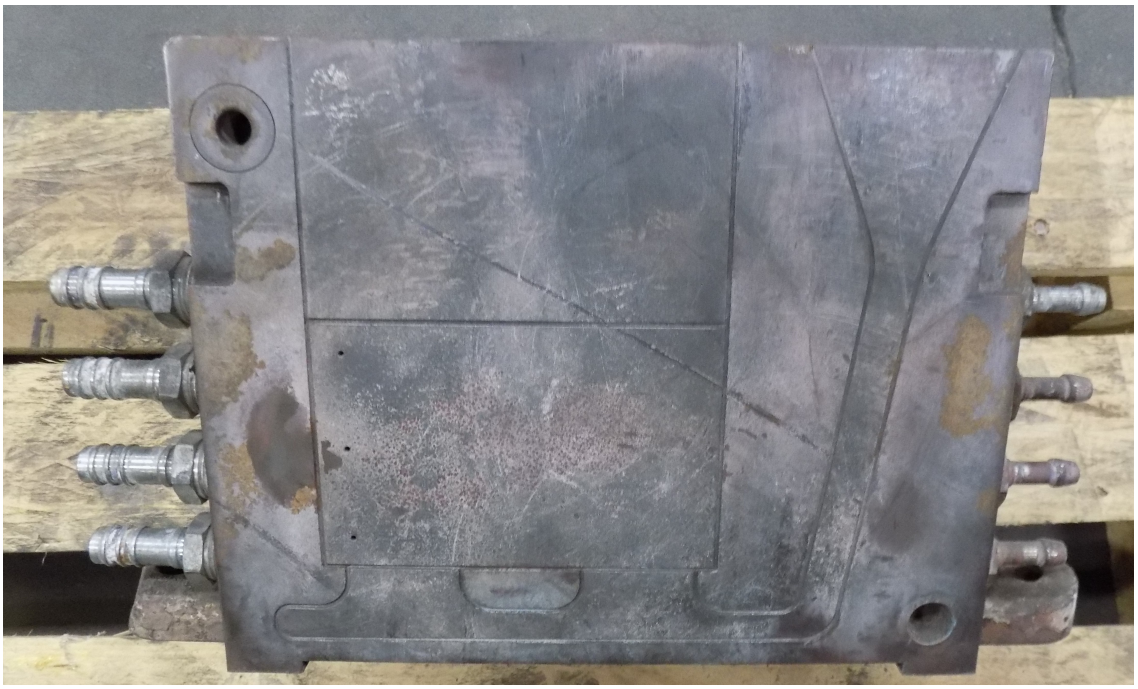

Figure 6: Linamar Mold: Flat Geometry Side.

Figure 7: Linamar Mold: Complex Geometry Side.

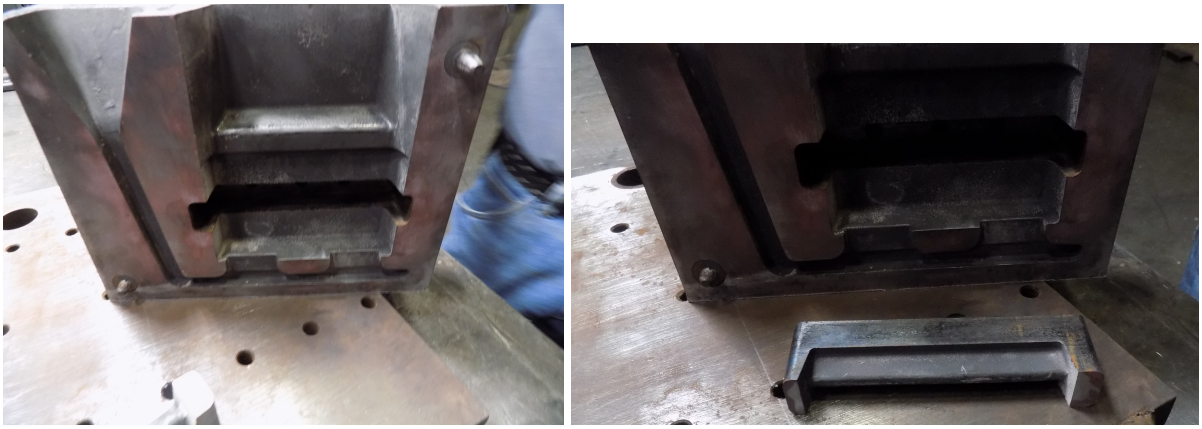

Figure 8: Linamar Mold: Insert Removed from Complex Geometry Side.

To increase the temperatures recorded with the new insert, four thermocouples were added as shown in Figure 9 with two thermocouples 2.54 mm (0.100”) from the casting surface and the other two thermocouples 6.35 mm (0.250”) from the surface. Unfortunately, the original Linamar insert had only one thermocouple and one corresponding exit for the thermocouple in the large mold side (Figure 10). Since the Linamar mold was on loan to ATEK, no permanent changes to the mold could be made, so channels had to be machined into the new insert to accommodate the thermocouples. These channels led to the existing thermocouple exit through the mold side as shown in Figure 11.

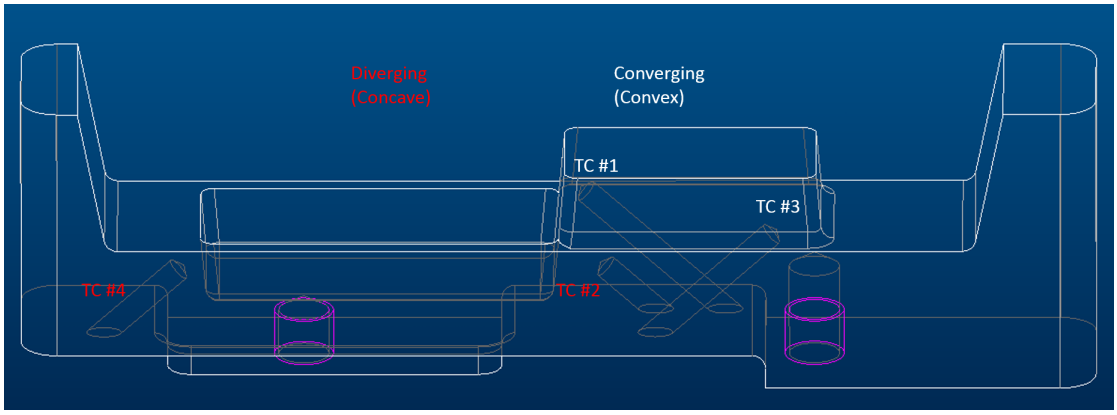

Figure 9: Linamar Mold: Thermocouple locations.

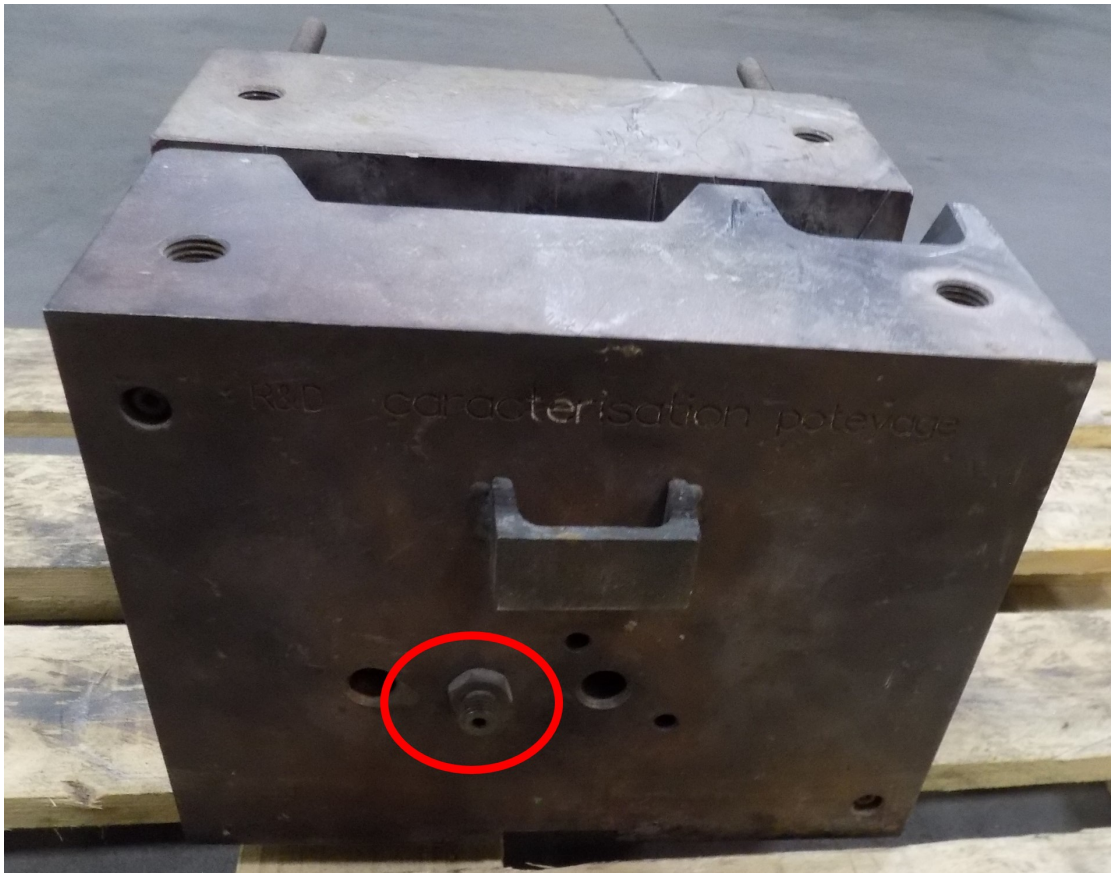

Figure 10: Linamar Mold: (Red) Existing Thermocouple Exit.

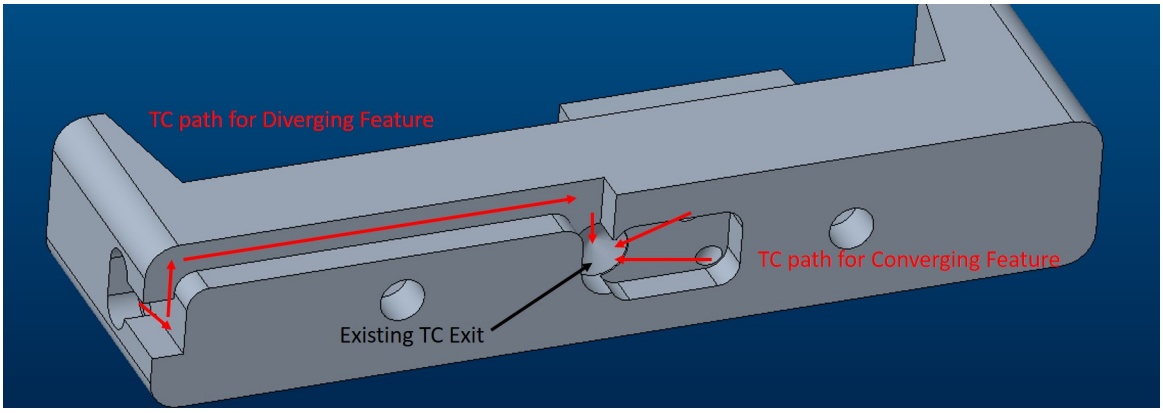

Figure 11: New Insert: (Red Arrows) Thermocouple Paths (Black Arrow) Existing Thermocouple Exit.

Wedge Mold with Fiber Optics

In addition to the Linamar mold, a separate mold was used to perform the fiber optic trials at Missouri University of Science and Technology. The overall mold design was based on an existing mold at ACRC-WPI. In function, four wedge inserts slide between two angle plates held in a grooved base. The wedges are tapered so when inserted into the mold the two angle plates are held in position as shown in Figures 12. The overall size of the Wedge mold was 312 mm wide by 178 mm tall by 102 mm wide (12.28" x 7.01" x 4.02"). A new mold variation was designed and machined, so the mold elements critical to the measurement of the interface coefficient (wedges) could fit within the operational window of ATEK's robotic mold spray booth. Additionally, two 1.27 mm (0.050") holes were drilled through the wedges to accept the steel encased fiber optic wires. Inherently, fiber optics can drastically increase the number of temperature measurements with recordings taken every 0.65 mm.

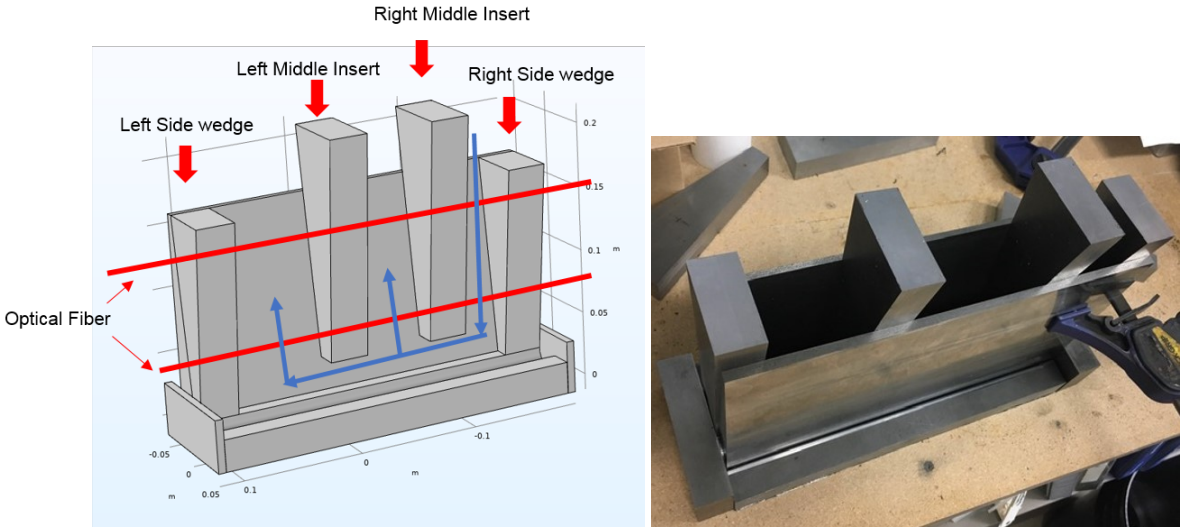

Figure 12: ACRC Wedge Mold: (Left) Individual Wedge Mold Components with blue arrows indicating metal flow during mold filling (Right) Assembled Wedge Mold.

Casting Trials

Two sets of casting trials, one with each mold, were performed one in a production setting and the other performed in a laboratory environment. Even through the locations were different, care was taken in both trials to minimize variation in mold and metal temperatures through consistent cycle times, mold preheat, and alloy selection.

Linamar Mold at ATEK

The new Linamar insert was fitted with four Type K thermocouples, which were fed through the outer mold wall. Gently, the insert was slid into the outer mold wall and bolted into place. The exterior mold halves were spot welded onto a movable metal table with pictures of the assembled mold shown in Figure 13. After the insert was installed, the table was moved near a holding furnace; preheated to at least 316°C (600°F) using a natural gas torch. While the mold was preheating, the aluminum melt furnace temperature was raised to 743°C (1370°F), fluxed, and degassed. Prior to pouring the first casting, a metal chemistry disc was taken and measured using a SPECTROMAX spectrometer.

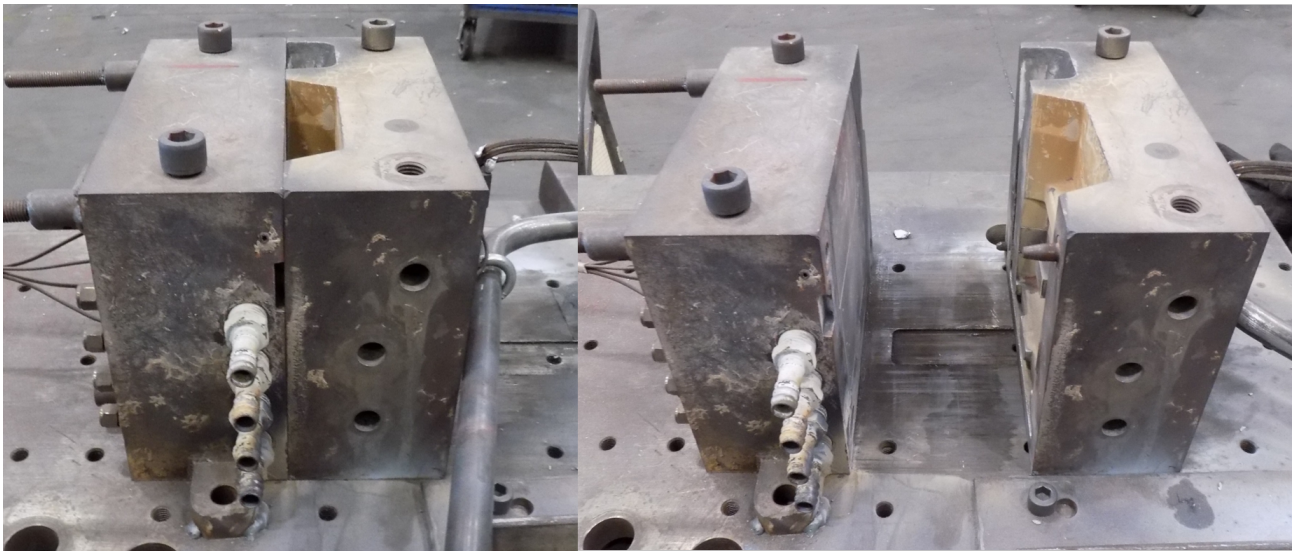

Figure 13: Linamar Mold: (Left) Mold in Closed Position (Right) Mold in Open Position.

With four of the five Linamar mold casting trials, 320 aluminum alloy was used but A356 alloy was used for one casting trial. Since these trials were run in a production facility, the alloys were selected based on availability, but both alloys are quite common permanent mold alloys. A356 is probably the most popular permanent mold alloy with silicon and magnesium alloying elements. While 320 is a variant of 319, which is another common permanent mold alloy, based on silicon and copper alloying elements. For comparison, the liquidus for A356 is 613°C (1140°F) while liquidus for 319 (comparable to 320) is 604°C (1120°F) [50]. With a melt holding temperature of 743°C (1370°F), there was 139°C of superheat with 320, and 130°C of superheat with A356 for a difference of 9°C (16°F).

Once the mold was preheated and the melt was at temperature, the metal was hand ladled into the mold. During the trials, insert temperatures were recorded using a PICO PP222 data-logger

and associated software. The metal temperature in the holding furnace was not recorded but was maintained at a steady 743°C (1370°F) in the furnace using an internal thermocouple with the same furnace temperature used for both alloys. During the entire Linamar mold trial, 200 castings were produced to measure the changes in heat transfer coefficient as the coating wears. Since this was not a tool designed for production use, it did not have an in-built ejector system to cleanly remove the casting from the die, which minimizes premature coating wear. As shown in Figure 14, a vibrator was attached to the complex geometry side to aid casting removal. Due to the production availability, all 200 castings could not be made in the same trial. The castings were produced over five separate trials with the casting totals for each trial shown in Table I. Pictures of a complete casting with the new insert design can be seen in Figure 15.

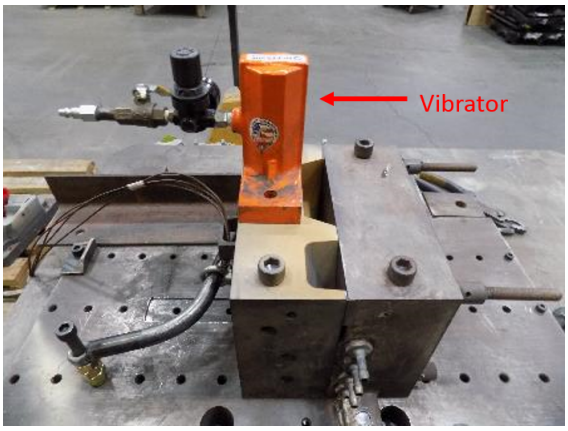

Figure 14: Linamar Mold: Vibrator (orange) attached to mold.

Table I: Linamar Mold: Standard Mold Coating Cast Trials.

Trial	Date	Alloy	Casting Shots	Cumulative Casting Shots
1	10/30/2020	320	29	29
2	11/4/2020	320	35	64
3	1/13/2021	320	47	111
4	1/27/2021	A356	51	162
5	2/19/2021	320	38	200

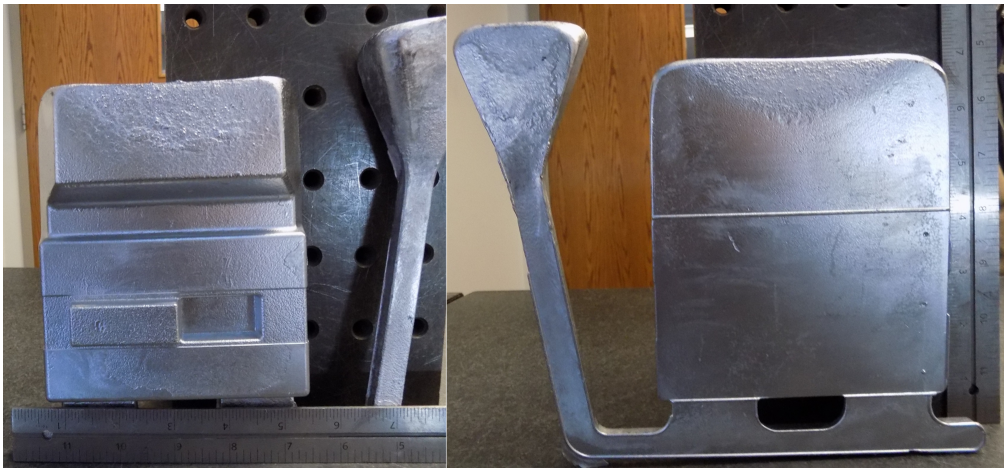

Figure 15: Linamar Mold: (Left) Complex Geometry Side of Casting (Right) Flat Geometry Side of Casting.

For each Linamar trial, the similar process was repeated with the mold preheated, insert temperatures recorded, and the metal chemistry recorded with all the chemistries shown in Table II. Starting after Trial #2, the coating thickness was measured on the insert's top flat as shown in Figure 16 using an Elcometer. Due to the measurement footprint of the Elcometer, the specific mold areas nearest to the thermocouples could not be measured. The top flat was the only area on the insert accessible for measurement.

Table II: Linamar Mold: Standard Mold Coating Trials Metal Chemistry at start of each Trial [51].

Trial	Date	Alloy	Si	Fe	Cu	Mn	Mg	Ti
1	10/30/2020	320	6.92	0.18	3.97	0.168	0.264	0.109
2	11/4/2020	320	7.2	0.1815	3.51	0.178	0.322	0.1097
3	1/13/2021	320	7.1	0.239	3.4	0.2	0.354	0.105
4	1/27/2021	A356	7.07	0.118	0.185	0.0115	0.329	0.135
5	2/19/2021	320	7.31	0.3	3.36	0.185	0.358	0.138
Alloy Ranges per ASM Handbook Volume 15								
		320	5.0-8.0	1.2 max	2.0-4.0	0.8 max	0.05-0.6	0.25 max
		A356	6.5-7.5	0.2 max	0.2 max	0.1 max	0.25-0.45	0.2 max

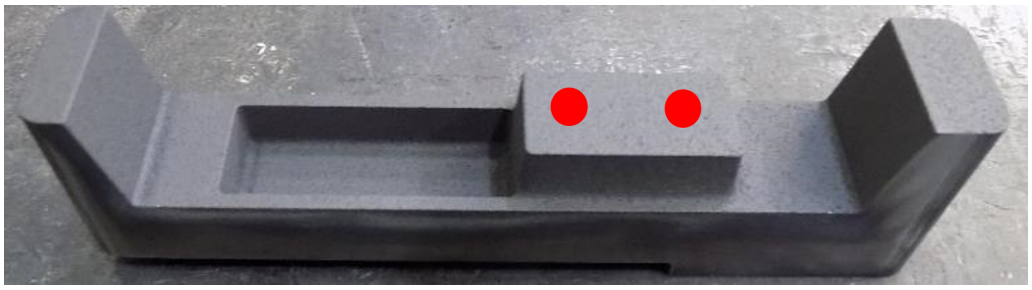

Figure 16: Linamar Mold: (Red) Elcometer Measurement Locations.

Wedge Mold at M.U.S.T.

Fiber Optic casting trials were performed at Missouri University of Science and Technology (M.U.S.T.) in collaboration with Dr. R. O'Malley's research group. While the Linamar trials produced 200 castings, the fiber optic trials using the wedge mold only produced two castings because the fibers had to be reset for each unique casting. Like the Linamar trials A356 was the alloy used, the mold was hand ladled, and the molds were preheated to 300°C (572°F) but in the fiber optic trials preheat was performed by hand torch and the pouring temperature was 720°C (1328°F). The signals from the fiber optics ran through a complex series of couplers and circulators as shown in Figure 17, which also shows the position of the fiber optics in the Wedge mold.

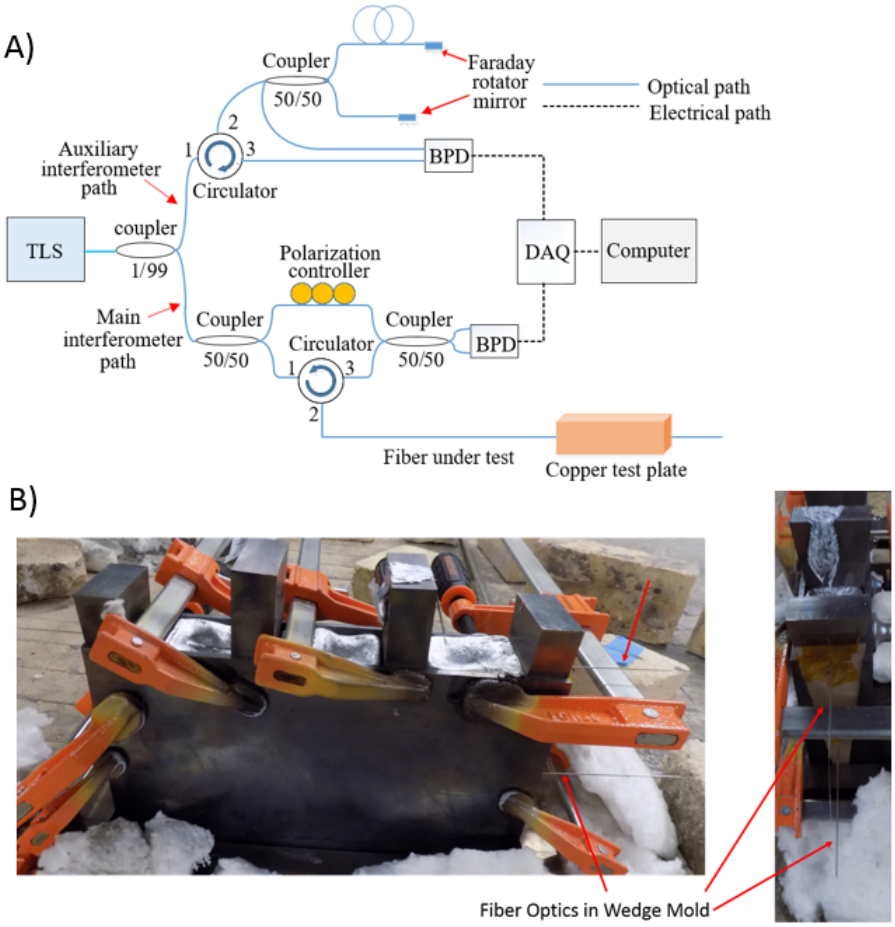

Figure 17: Wedge Mold: (A) Schematic of Fiber Optic Temperature Path (B) Position of Fiber Optics in Mold.

4.2 Simulation of Linamar Mold

Solidification simulations were run using EKK Capcast software. Before the experimental trials were performed, the Linamar mold was run to find the average process settings that were used to setup simulations, which included 10 seconds fill time, 250 second solidification cycle, and 743C (1370°F) metal temperature. These simulation settings were defined before the trial, so

simulations could be run in conjunction with casting trials. For the initial simulations, HTC of 837 $Wm^{-2}K^{-1}$, which is the baseline value used in the software, was used. The heat transfer coefficient was changed in increments of 250 $Wm^{-2}K^{-1}$ from 339 to 2089 $Wm^{-2}K^{-1}$ from the baseline value during subsequent simulations. The temperature values for the four thermocouples were recorded during the simulations. The spread of the simulated temperatures was overlaid with the experimental values from a steady state new coating casting cycle (Shot #22) from the first casting trial. Then, the temperature values between the steady state new coating (Shot #22) were compared with the temperatures recorded during Shot #180, which represented the worn coating. For the simulated values, the average absolute error between the calculated and experimental temperatures (Equation 25) was used to quantify the differences between the simulated and experimental values.

$$\bar{X}_{Error} = \frac{1}{n}\Sigma_{i=1}^{n}|T_{Simulated} - T_{Experimental}| \tag{25}$$

Based on the error values between the experimental and simulated temperatures, it was determined a single HTC value was not sufficiently accurate to simulate the experimental temperatures. Initially, a two-step HTC value was used for thermocouple #2 with the values used shown in Table III, but then a three-step heat transfer coefficient was used. Three-step HTC values were modeled for thermocouples #2 and #3, which represent both casting geometries at a depth of 6.35mm (0.250”). Due to time limitations, it was not feasible to run three step simulations for all four insert thermocouples. Since there were temperature differences between thermocouples #2 and #3, different HTC values were used to simulate each experimental temperature. To model a three-step heat transfer coefficient value, the initial Metal Hold step was broken into three segments. The three step HTC values modeled for TC#2 are in Table IV, while the values used for TC#3 are displayed in Table V.

Table III: Linamar Mold: two-step HTC Values ran for TC2.

	Step 1		Step 2	
Simulation	Time(s)	HTC ($W/m^2.K$)	Time(s)	HTC ($W/m^2.K$)
1	50	1086	200	200
2	30	1086	220	200
3	40	1086	210	200
4	50	837	200	200
5	50	750	200	200
6	50	650	200	200
7	50	550	200	200
8	50	600	200	200
9	50	610	200	200

Table IV: Linamar Mold: Three Step HTC Values ran for TC2.

	Step 1		Step 2		Step 3	
Simulation	Time(s)	HTC ($W/m^2.K$)	Time(s)	HTC ($W/m^2.K$)	Time(s)	HTC ($W/m^2.K$)
1	50	610	20	400	180	200
2	50	610	20	400	180	100
3	50	610	50	400	150	100
4	50	610	30	400	170	100

Table V: Linamar Mold: Three Step HTC Values ran for TC3.

	Step 1		Step 2		Step 3	
Simulation	Time(s)	HTC ($W/m^2.K$)	Time(s)	HTC ($W/m^2.K$)	Time(s)	HTC ($W/m^2.K$)
1	50	610	20	400	180	200
2	50	610	20	400	180	100
3	50	610	50	400	150	100
4	50	610	30	400	170	100

4.3 Design of Geometry

The new insert design had two geometric features, one creating a converging heat flow into the die (convex die surfaces) and the other a diverging heat flow (concave die surfaces), as shown in Figures 18 and 19. The left most geometric feature is a negative in the insert creating a positive feature in the casting. Contrarily, the right geometric feature is a positive in the insert making a negative feature in the casting. As the casting solidifies, it will tend to shrink onto the positive tooling feature enabling casting to mold contact for a longer period. At the same time, the casting will "pull away" from the negative tooling feature as it solidifies, leading to less heat transfer. Ideally these two features would be isolated from each other so no overlap in heat flow would occur, but due to the limited size of the insert this was not possible.

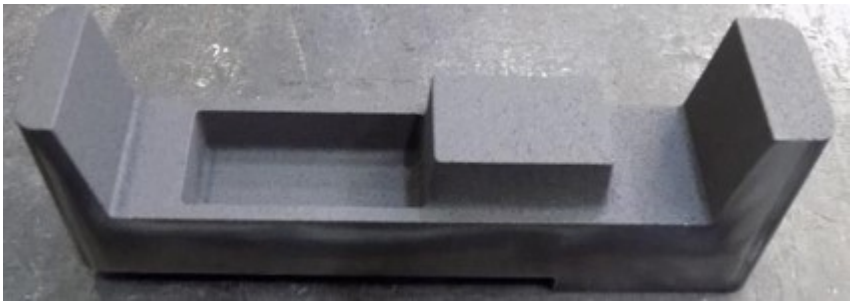

Figure 18: New Linamar Insert Design: (Left) Diverging Heat Flow Feature (Right) Converging Heat Flow Feature.

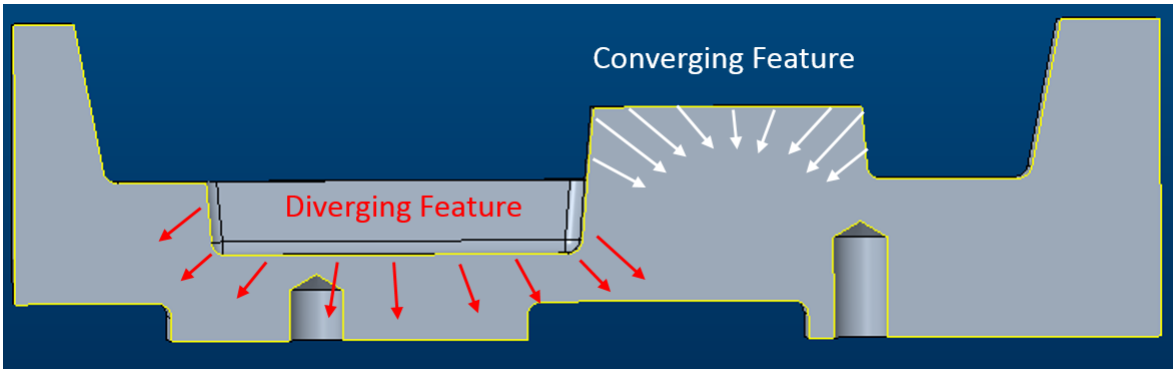

Figure 19: New Linamar Insert Design: (Left) Diverging Heat Flow Feature (Right) Converging Heat Flow Feature.

4.4 Mold Coating

Defining a Standard Mold Coating

A primary purpose of this work was to measure the impact of mold coating wear on heat transfer coefficient, but it is difficult to define what is a standard mold coating let alone what signifies a worn mold coating. As previously mentioned, each foundry will use coatings with different compositions in varying combinations; the same foundry will use different coatings for different castings so there is no standard universal mold coating. When a coating starts to produce an unacceptable number of defects, the coating is considered worn, which must be proven out for each casting.

A high production industrial example was used to define the standard coating and worn coating. ATEK Metal Technologies is a permanent mold and low-pressure permanent mold foundry in NE Iowa, which primarily produces castings for power sports. The main casting produced is a cylinder head for motorcycles with yearly volumes well over 200,000. This specific cylinder head has cast cooling fin segments achieved by assembled tool segments known as “lamination packs”, which are shown in Figure 20. These packs must be disassembled and resprayed frequently (after approximately 200 casting cycles) to prevent defects such as spray chips, misruns, and “drags” (scrape marks on castings occurring during ejection from the mold).

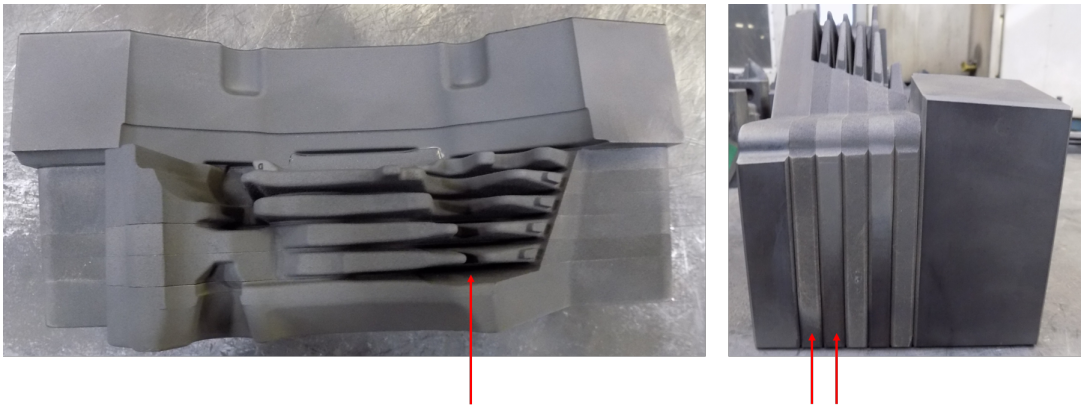

Figure 20: (Left) Top view of Assembled Lamination Pack (Right) Side view of Assembled Lamination Pack with Individual Laminates highlighted.

To increase efficiency and reliability, the individual laminates (lams) are coated in a robotic spray booth (Figure 21) that heats laminates to roughly 260°C (500°F) and sprays multiple layers of three different coatings. In practice, most mold coatings are applied manually with a trained operator leading to variations in the thickness of the applied coatings. These variations can easily cause more air to become trapped in coating or vary layer thickness causing changes in heat transfer coefficient. The coatings applied to the lams are an insulating coating, a texture coating, and a release coating. The composition and applied thickness will vary across industry, but the three coatings types (insulating, texture, and release) will be used.

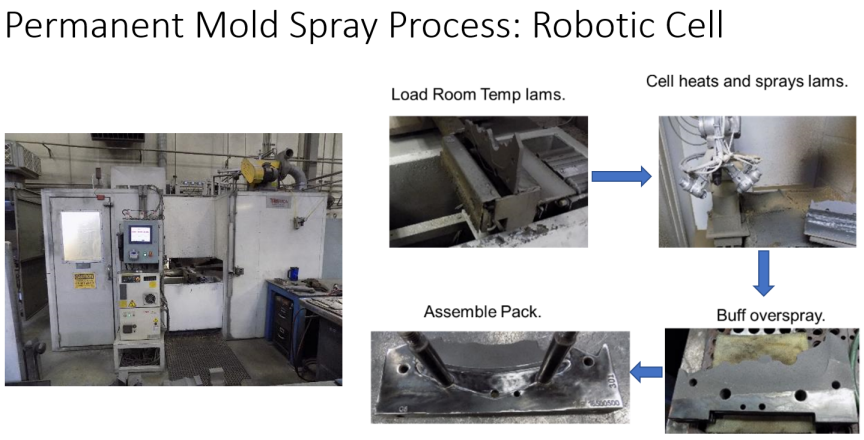

Figure 21: Robotic Spray Process for a Standard Lamination Insert.

To define the standard coating, a laminate was run through robotic spray booth with the regular process. The composition and applied thickness, as measured with an Elcometer, for the standard coating are shown in Tables VI and VII, which will vary across industry. A second lam was taken from a lamination pack that had been ran for roughly 23 hours and was waiting to be resprayed. The

second lam represented a worn coating, and both lams were sent to WPI for microscopic analysis in collaboration with Dr. S. Darvish as shown in Figure 22. With the new coating, primarily the graphite outer layer can be seen but with wear the lower brown and white layers become visible.

Table VI: Coating Compositions.

Coating Name	Color	AKA	% Sodium Silicate	% Vermiculite	% Quartz (SiO2)	% Mica	% Graphite
BONDERITE L-CA 193	White	193 White	-	-	1-5	5-10	-
BONDERITE L-CA CG-104	Brown	104 Brown	10-30	10-30	1-5	-	-
BONDERITE L-GP PRODAG	Black	Graphite	-	-	0.1-1	-	10-30

Table VII: Coating Thickness for Standard Coating.

		Cumulative Thickness	
Coating Name	Spray Passes	Millimeter	Mils
193 White	4	0.10-0.15	4-6
104 Brown	3	0.18-0.2	7-8
Graphite	2	0.23-0.25	9-10
Overall Coating Thickness		0.25-0.36	10-14

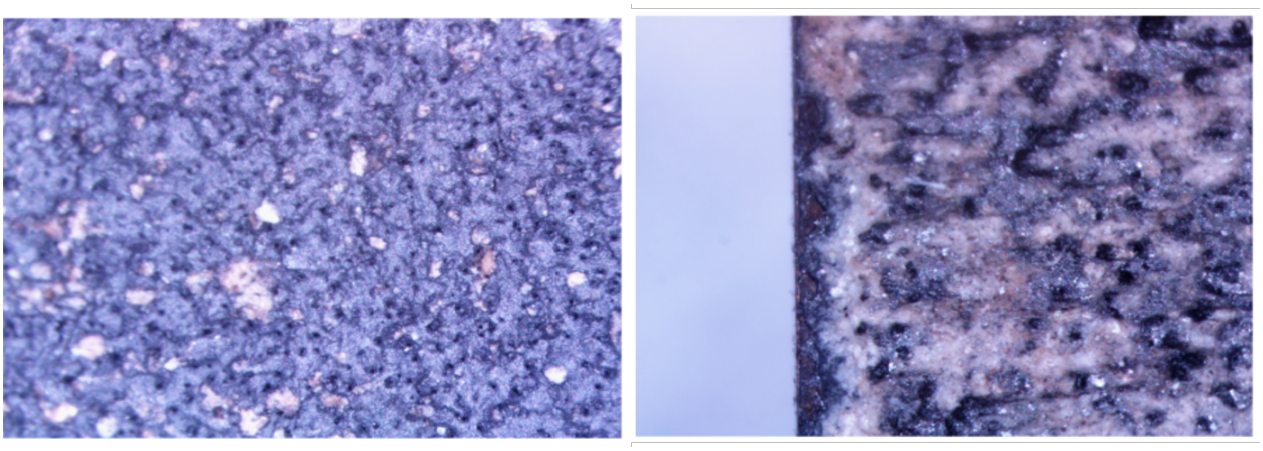

Figure 22: Coating Thickness for Standard Coating measured at WPI. (Left) Microscope Picture of Lam with New Standard Mold Coating (Right) Microscope Picture of Lam with Worn Standard Mold Coating.

Coating for Casting Trials

The new Linamar mold insert and Wedge mold center inserts (wedges), which contact the fiber optic wire, were coated in ATEK's robotic spray booth with the process steps for a standard lamination insert shown in Figure 21. The inserts were cleaned of any oil to ensure proper coating adhesion and preheated to roughly 260°C (500°F) before entering the booth. The robotic spray

booth applied three different mold coatings onto the insert with an overall thickness of 0.254-0.356 mm (10-14 mils). The composition of each coating is shown in Table VI, while the coating thickness per coating is given in Table VII. These data are representative of ATEK's standard coating used on a long running production part. The base and angle plates used in the Wedge mold, which did not contact the fiber optic wire, were hand sprayed using the standard mold coating with an overall thickness of 0.254-0.356 mm (10-14 mils).

5 Results and Discussion

5.1 Temperature Profiles during Linamar Mold Trials

Since the standard coating trial had to be performed over five separate casting trials, it was critical the temperature values over the trials were consistent. All the insert temperatures recorded during the trials are shown in Figures 23 - 27. In all A356 trials once a steady mold temperature was reached, the insert temperatures varied from 750°F to 950°F (399°C to 510°C) with consistent distribution of temperatures throughout the 320 trials. The temperature range for Trial #4 (Figure 26) was slightly different with the temperature values ranging from 800°F to 1000° F (427°C to 538°C) at steady state. The fourth trial used A356 alloy, while all the other trials used 320 alloy.

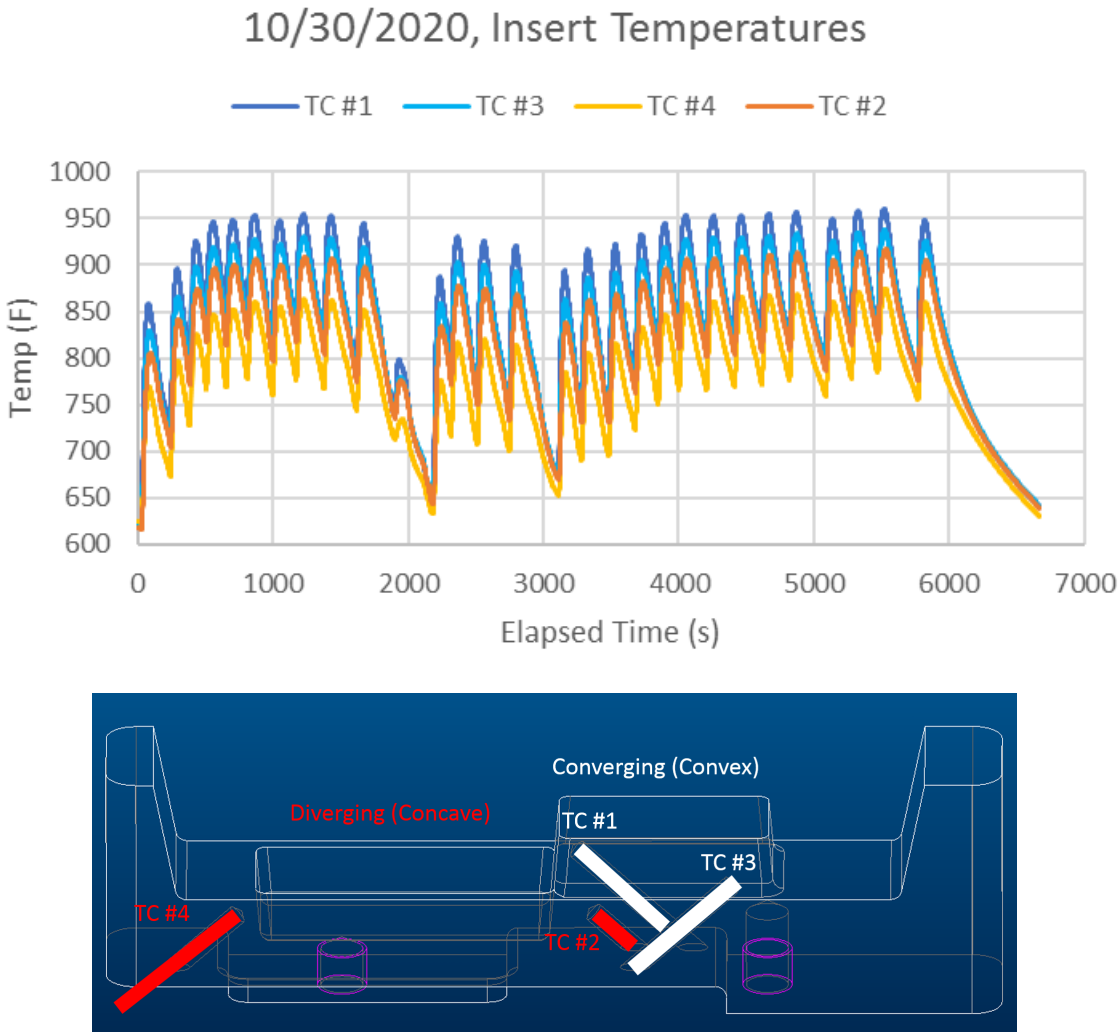

Figure 23: Linamar Mold: (Top) Trial 1 (10/26/2020) Thermocouple Temperatures (320 Alloy), (Lower) Thermocouple Locations.

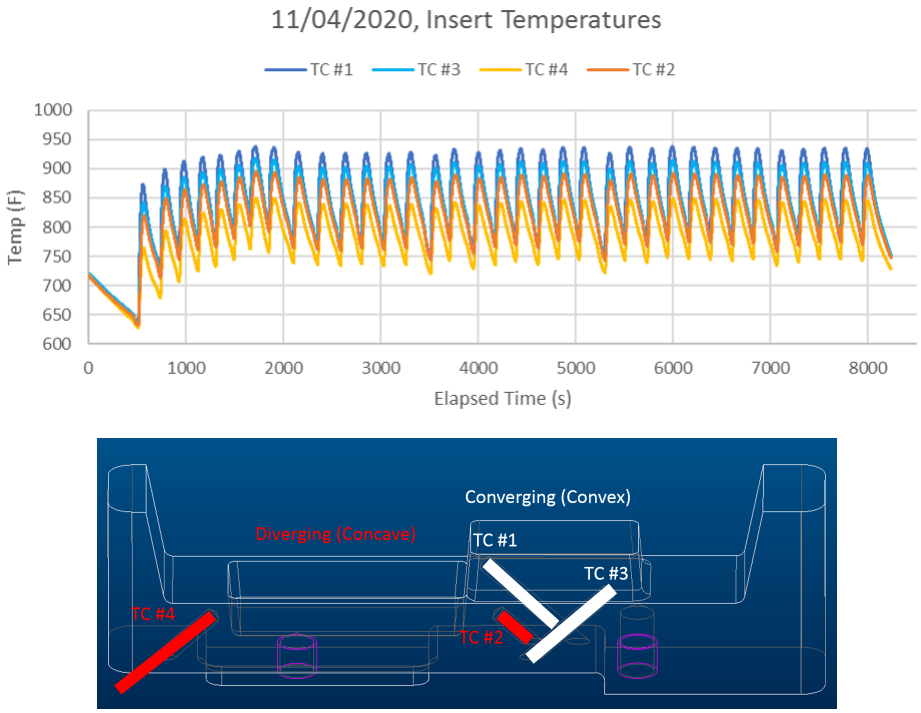

Figure 24: Linamar Mold: (Top) Trial 2 (11/04/2020) Thermocouple Temperatures (320 Alloy), (Lower) Thermocouple Locations.

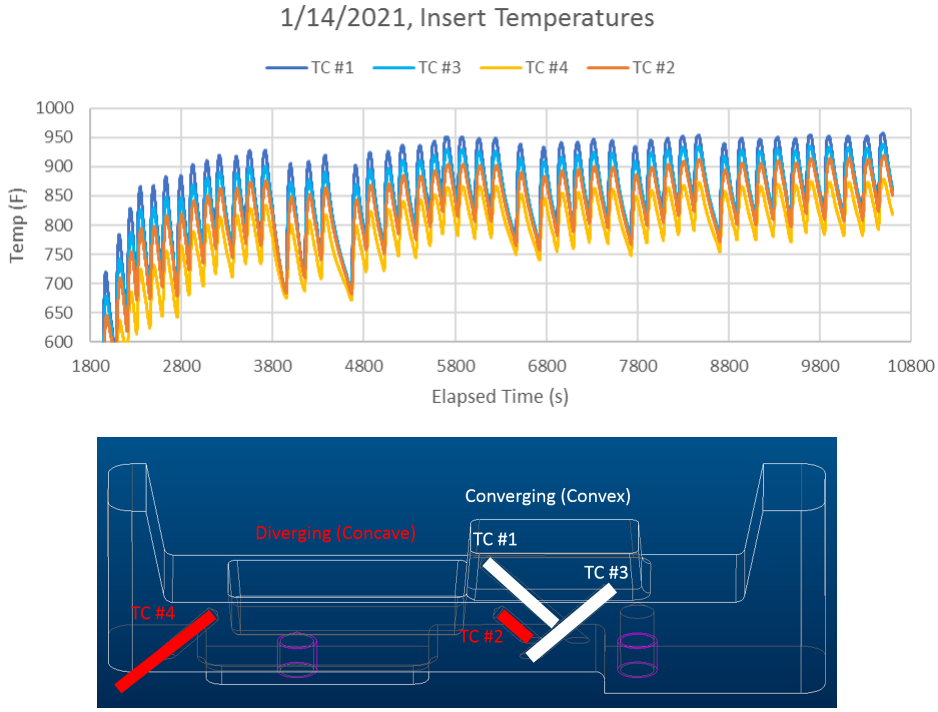

Figure 25: Linamar Mold: (Top) Trial 3 (1/14/2021) Thermocouple Temperatures (320 Alloy), (Lower) Thermocouple Locations.

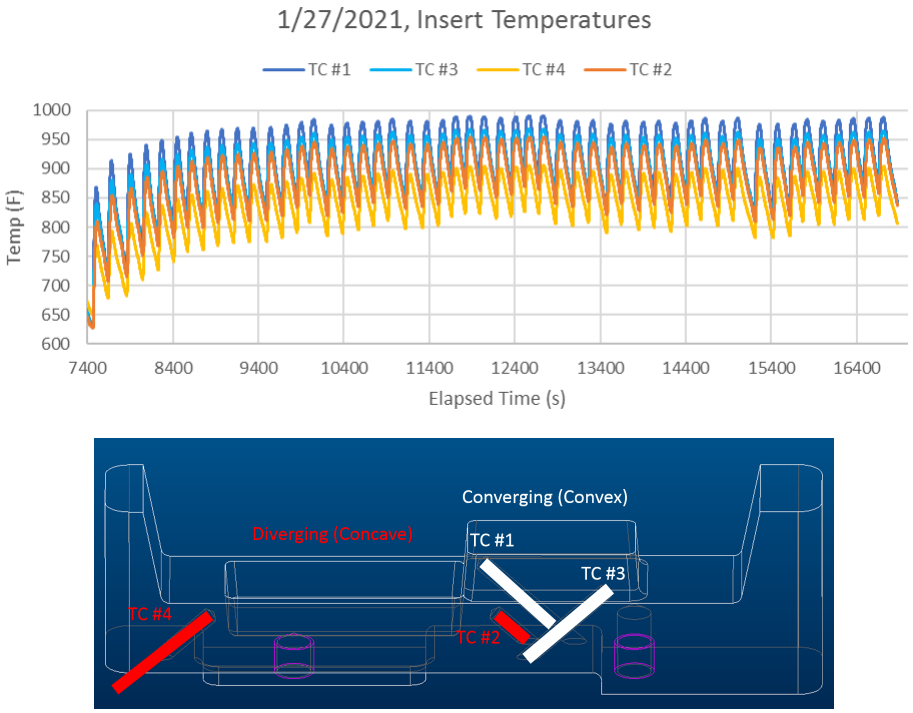

Figure 26: Linamar Mold: (Top) Trial 4 (1/27/2021) Thermocouple Temperatures (A356 Alloy), (Lower) Thermocouple Locations.

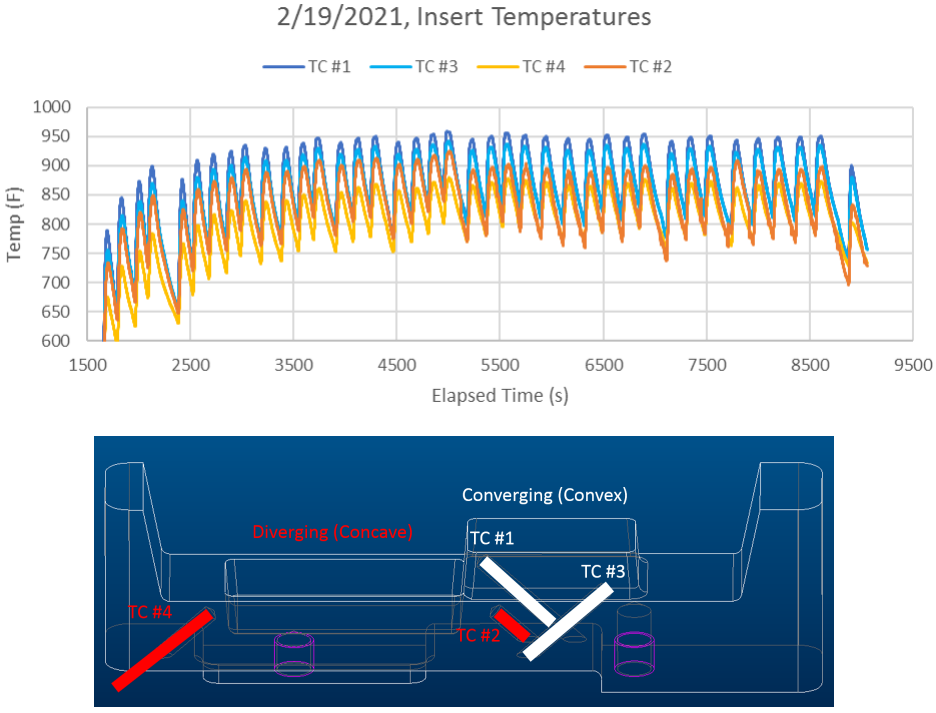

Figure 27: Linamar Mold: (Top) Trial 5 (2/19/2021) Thermocouple Temperatures (320 Alloy), (Lower) Thermocouple Locations.

In terms of individual temperature readings, TC#1 had the highest peak temperature of 950°F (510°C), and TC#4 had the lowest peak temperature of 860°F (460°C). TC#2's max value was 910°F (488°C), and 925°F (496°C) for TC#3. The largest difference in temperature was between TC#1 and TC#4, which were both 2.54mm (0.100") from the casting surface for the two different features. While TC#2 and TC#3 were more similar with both thermocouples 6.35mm (0.250") from the casting surface for the two features.

The low peak temperatures recorded at position TC#4, despite its closer proximity to the casting surface, requires some comment. It was located on the outer edge of the insert, adjacent to a concave feature in the mold, while the other three thermocouples were in the relative middle of the insert. It is likely the location of TC#4 with respect to casting geometry had a greater impact on its temperature response than its distance to casting surface. If distance to the casting surface was the only first order influence on TC#4's response, it should have recorded a higher peak temperature than TC#2 and TC#3.

Even with the differences in temperatures caused by the alloy, the overall pattern for each trial was similar. The insert temperature would start slightly lower between 600°F to 650°F (316°C to 343°C) and climb over 3 - 5 cycles to reach a steady temperature. Since the mold was operated by hand, there were fluctuations in temperature during each trial. These variations were caused by downtime during operation of the mold. Since the mold did not have an ejector system, the casting would stick in the mold so time would be lost removing it. A vibrator was used to help promote ejection, but the complex geometry added to the insert hindered ejection. Under normal production circumstances, graphite mold coating would be sprayed onto the offending tooling area, but this could not be used as it would have increased mold coating thickness.

5.2 HTC Simulations

Different approaches were taken to define realistic heat transfer coefficient values during simulations to accurately mold the standard coating model the standard mold coating as defined by the temperatures from Shot # 22, with a one-step (constant) heat transfer coefficient value being tried initially, followed by a two-step value, and finally a three-step heat transfer coefficient value.

Simulation with One-step HTC Values

All the simulated thermocouple readings using values of HTC ranging from 339-2089 $Wm^{-2}K^{-1}$ are shown in Figure 28 with the experimental values from Shot # 22 overlaid for each per thermocouple location. An overlay with just the closest simulation to the experimental value is shown in Figure 29. For TCs#1 and #2, the closest simulation to the experimental used a HTC value of 1086 $Wm^{-2}K^{-1}$. For TC#3, the most comparable simulation was 2089 $Wm^{-2}K^{-1}$ while 588 $Wm^{-2}K^{-1}$ was most like TC#4. Aside from the HTC simulations, all the thermocouple values followed the same pattern with a peak temperature value reached between 40-50 seconds followed by a gradual decline.

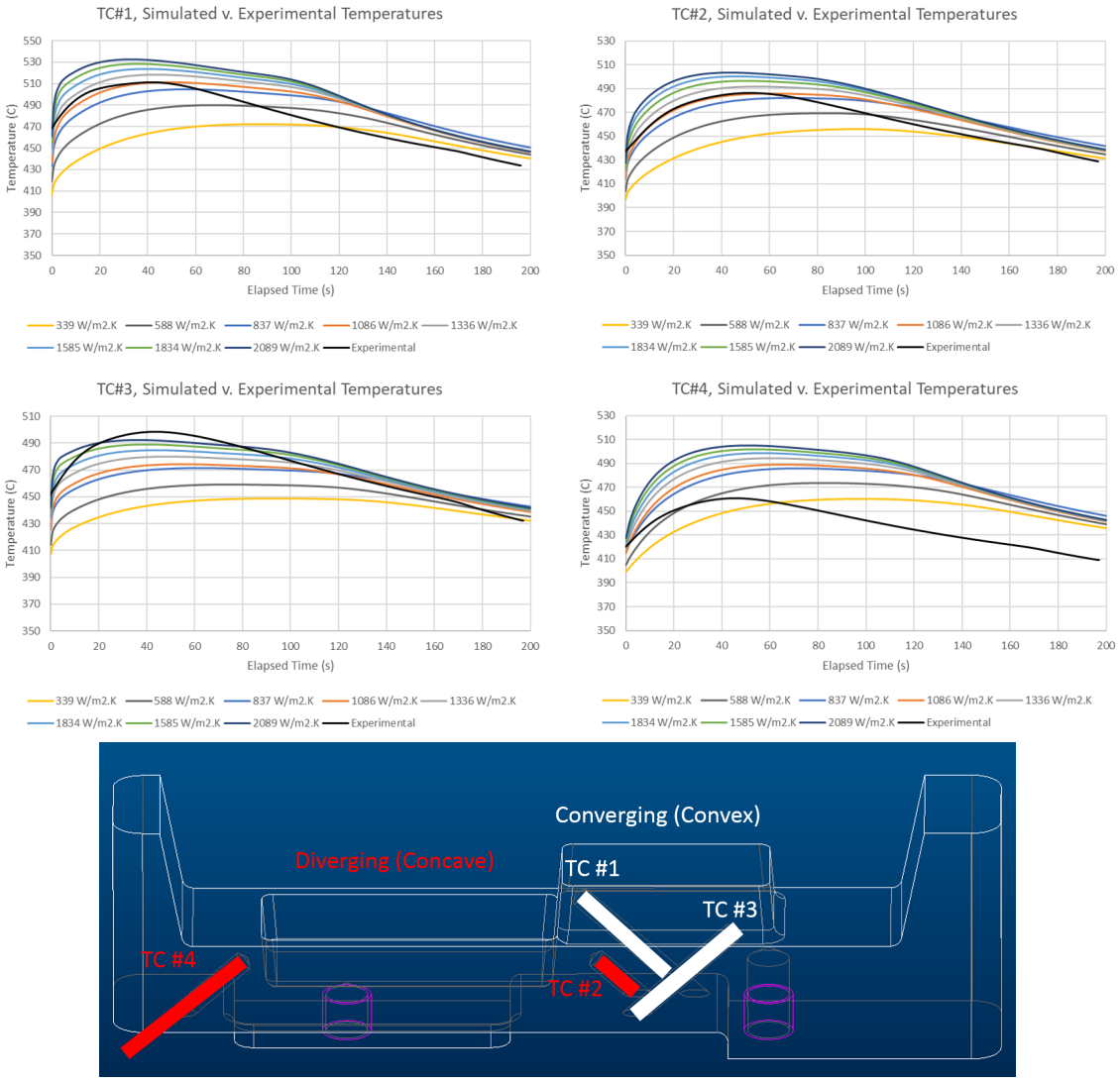

Figure 28: Linamar Mold: (Above) Trial 1 TCs#1-4 v. All Simulated Values, (Below) Thermocouple Locations.

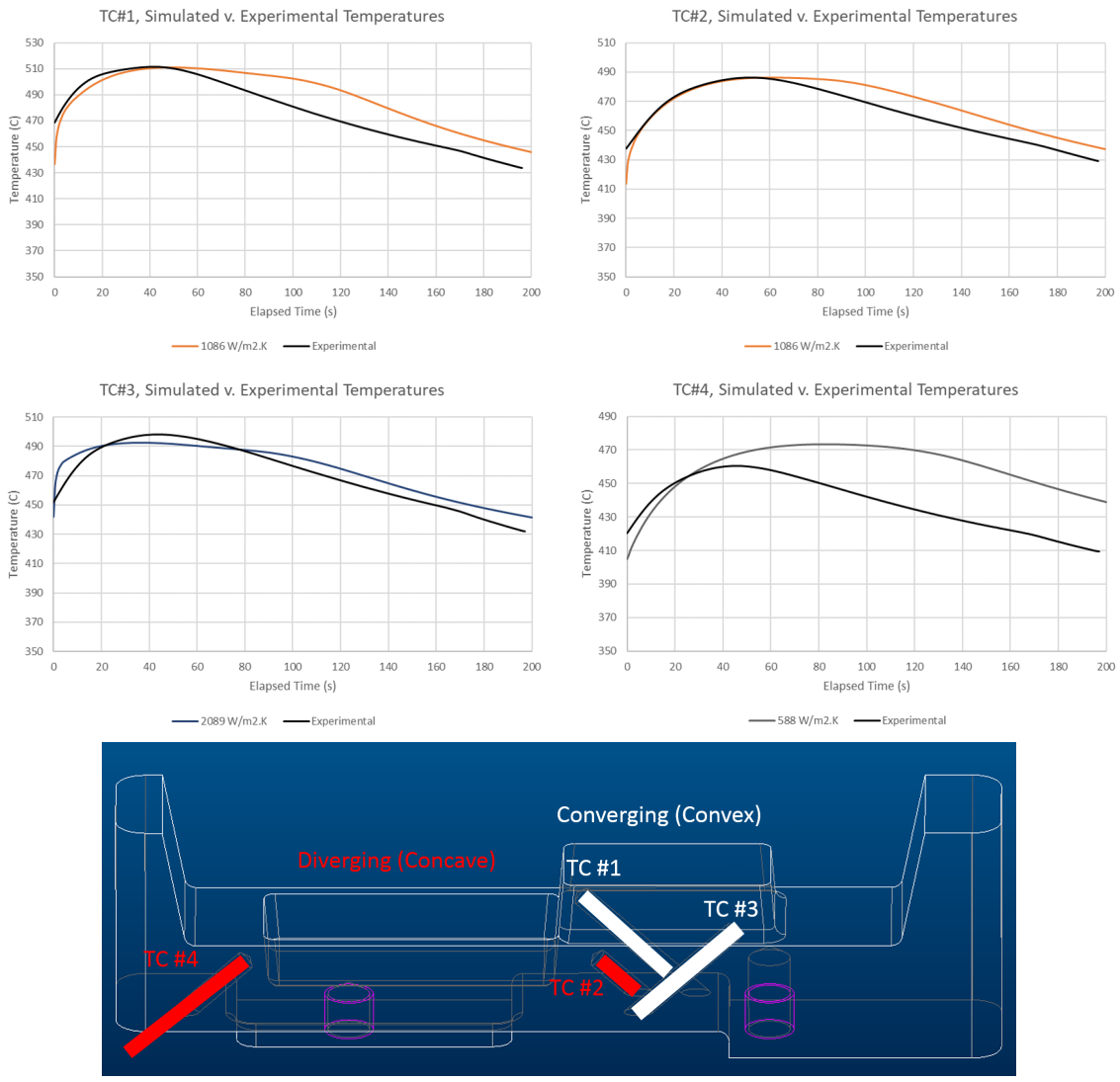

Figure 29: Linamar Mold: (Above) Trial 1 TCs #1-4 v. Closest Simulation, (Below) Thermocouple Locations.

The average absolute error values between all the simulated and experimental values are shown in Table VIII with the lowest values highlighted in green. For TC#1, the lowest average error was 13.05°C, and 19.03°C for TC#4. Both thermocouples are within 2.54mm (0.100") of the casting surface. TCs#2 and #3 were both 6.35mm (0.250") from the casting and had an average error value of 7.17°C and 6.02°C. Visually TC#3 did not align with the simulated value in a similar fashion as the other thermocouples, which showed more overlap for a longer time. TC#4 was only close to the simulated value during the beginning of the cycle and showed an increasing gap through the rest of the cycle.

Table VIII: Linamar Mold: Shot #22 HTC Average Absolute Error (Top) Over Entire Cycle (Bottom) First 50 seconds of Cycle.

Over Entire Cycle

Average Absolute Error	339 W/m2.K	588 W/m2.K	837 W/m2.K	1086 W/m2.K	1336 W/m2.K	1585 W/m2.K	1834 W/m2.K	2089 W/m2.K
TC#1	22.50	16.22	15.56	13.05	15.61	18.66	21.08	23.03
TC#2	18.34	11.09	9.52	7.17	10.31	15.43	13.15	17.32
TC#3	29.54	20.63	13.50	10.65	8.19	6.69	6.04	6.02
TC#4	19.03	22.87	32.51	33.36	36.96	39.77	42.03	43.90

First 50s of Cycle

Average Absolute Error	339 W/m2.K	588 W/m2.K	837 W/m2.K	1086 W/m2.K	1336 W/m2.K	1585 W/m2.K	1834 W/m2.K	2089 W/m2.K
TC#1	52.63	31.16	12.18	4.19	6.41	12.81	18.27	22.85
TC#2	39.24	23.12	7.15	1.94	6.63	16.82	12.13	20.90
TC#3	52.36	39.41	25.09	21.04	14.28	9.40	6.78	5.91
TC#4	15.97	5.40	13.87	18.17	24.42	29.70	34.19	38.07

Due to the increasing separation between the simulated and experimental values after 50 seconds, the average absolute error was calculated for just the first 50 seconds of the cycle, which is also shown in Table VIII. The lowest error values for all the thermocouples decreased with the highest error being 5.91°C for TC#3. The lowest error value became 1.94°C for TC#2. A direct comparison of the two sets of error values can be seen in Figure 30. TCs#2 and #4 both showed a roughly four-fold decrease from 19.03°C to 5.40°C and 7.17°C to 1.94°C. TC#1 dropped 68% from 7.17°C to 1.94°C. Uniquely TC#3 only showed an exceedingly small drop from 6.02°C to 5.91°C. This difference is likely caused by how TC#3 intersected the simulated HTC curve at multiple points. When only the first 50 seconds of the cycle were considered, there is a stark change in lowest error values, so it is logical something fundamentally changed at this point in solidification. This change is most likely the formation of an air gap which drastically reduces the heat transfer coefficient. Additionally, with the average absolute error above 5°C for the entire cycle, it is obvious a single HTC is not accurate enough to simulate the experimental values.

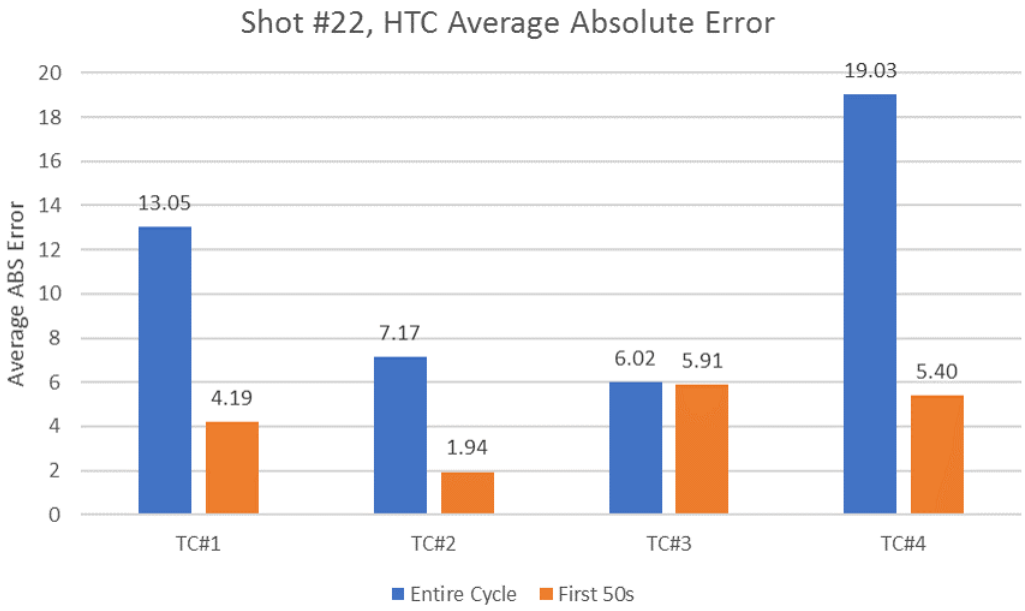

Figure 30: Linamar Mold: Shot #22 HTC Average Absolute Error Over Entire Cycle v First 50 seconds of Cycle.

Simulation with Two-step HTC Values

To reduce the absolute average error between the simulated and TC#2 experimental temperatures for Shot #22, nine simulations were run using a two-step heat transfer coefficient value with time dependent changes in HTC, which are shown in Figure 31. Simulation #9 was the closest to the experimental temperatures with a direct comparison shown in Figure 32. During the first 50 seconds, the heat transfer coefficient was 610 $Wm^{-2}K^{-1}$ and for the next 200 seconds the HTC was changed to 200 $Wm^{-2}K^{-1}$. Initially, the two stages simulations were run using a constant 1086 $Wm^{-2}K^{-1}$ HTC, which was the closest value in the one step process, but this resulted in simulated temperatures roughly 40°C above the experimental values. Additionally, when the HTC value transitioned at 30-50 seconds there was slight jog in the simulated temperatures, which was likely caused by the software.

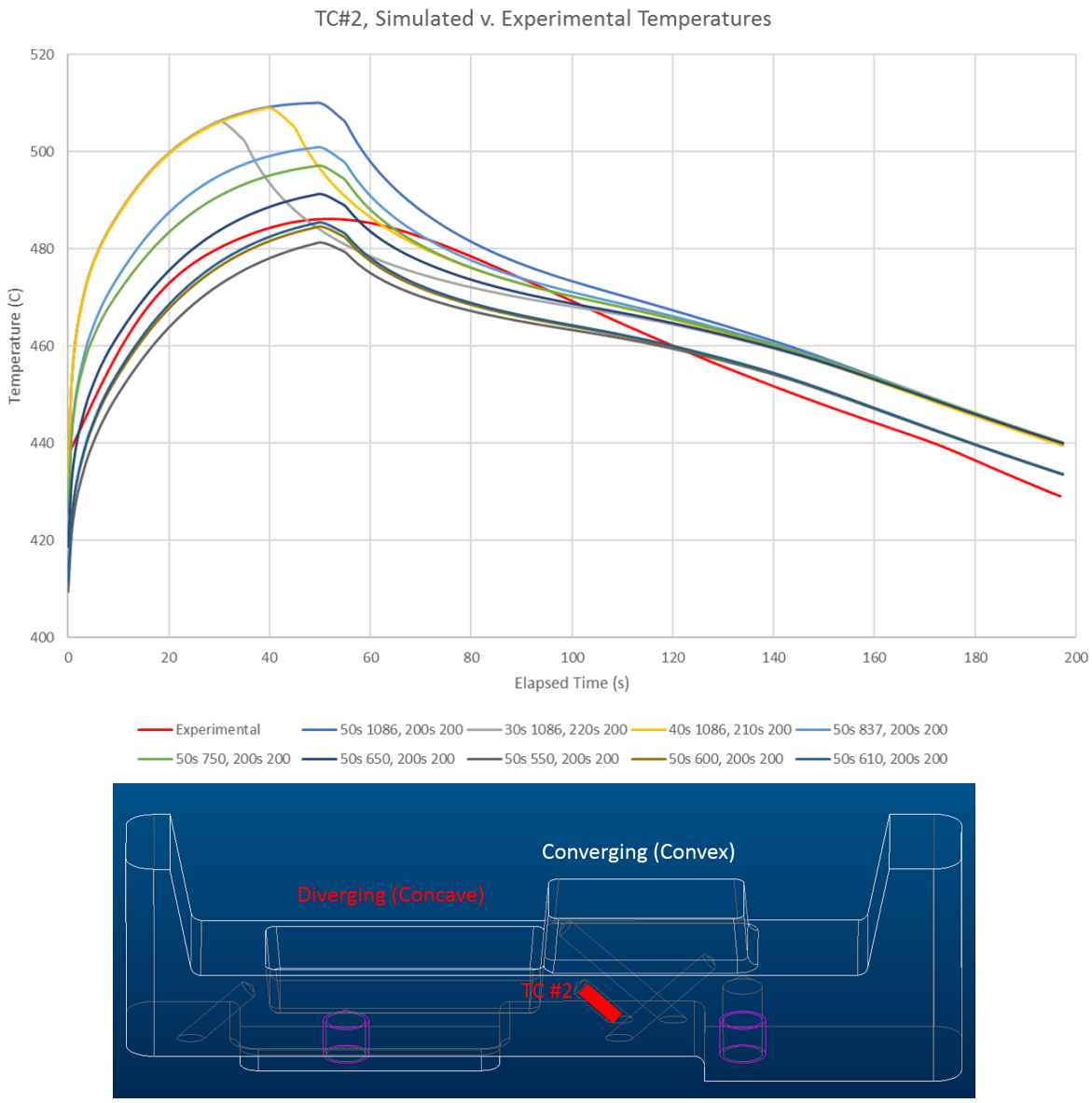

Figure 31: Linamar Mold: (Above) Shot #22 TCs #2 v. two-step Simulation, (Below) Thermocouple Location.

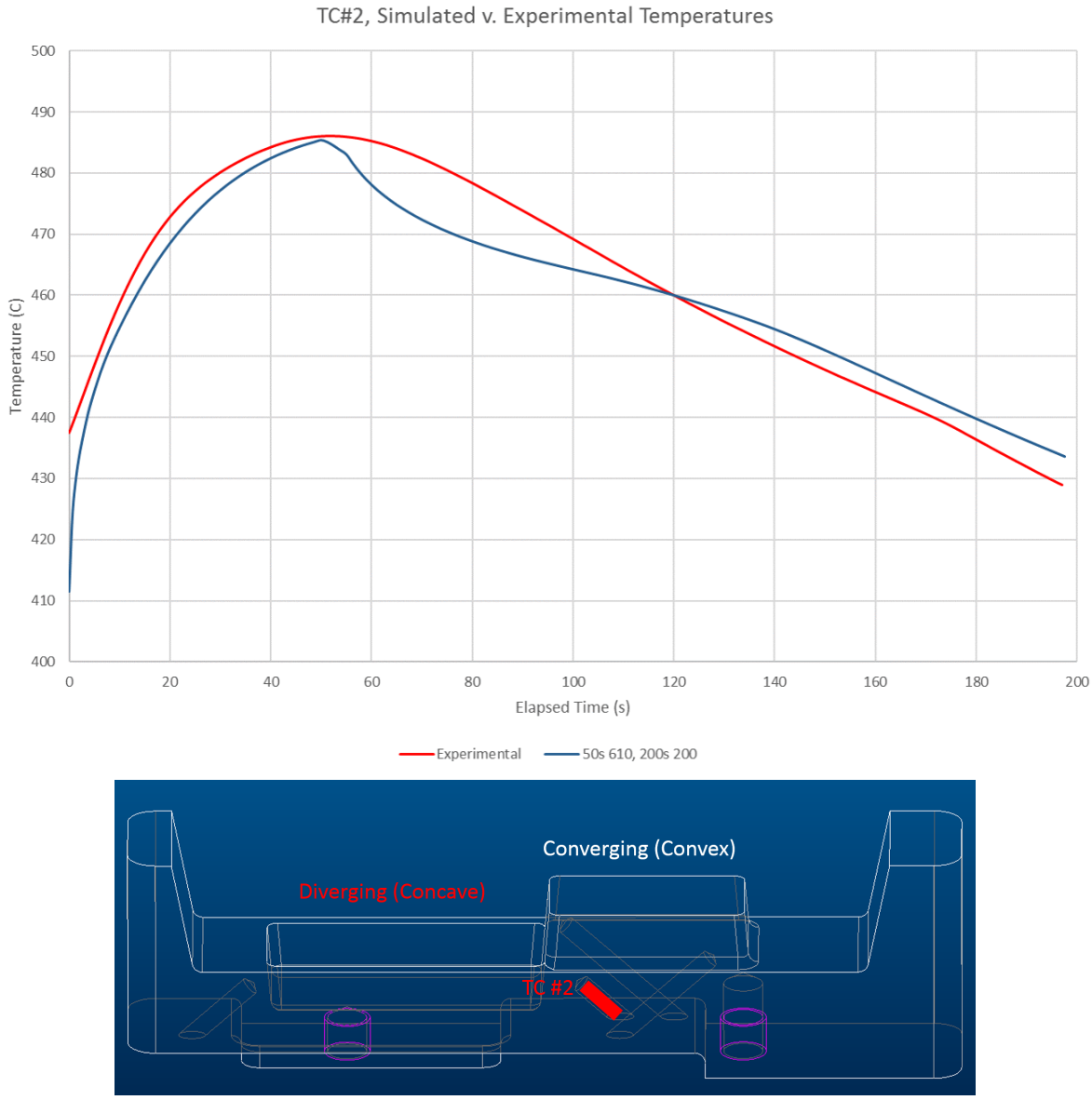

Figure 32: Linamar Mold: (Above) Trial 1 TCs #2 v. Simulation #9, (Below) Thermocouple Location.

Aside from the visual comparison, the average absolute error between the experimental and simulated values were calculated for each simulation as displayed in Table IX. The last simulation had the lowest error value of 4.38°C, while the first simulation had the error value of 12.70°C. Since 1086 $Wm^{-2}K^{-1}$ overshot the experimental temperatures, primarily the HTC value of the first step was changed during the simulations. As the HTC value was lowered, the error value decreased until the lowest HTC value of 610$Wm^{-2}K^{-1}$ was reached. As compared to the error value of the one step HTC of 7.17°C, the error value was reduced to 4.38°C with the two-step process.

Table IX: Linamar Mold: Shot #22 TC#2 with two-step HTC Value.

	Step 1		Step 2		
Two Step Simulation	Time (s)	HTC (W/m^2.K)	Time (s)	HTC (W/m^2.K)	Average Absolute Error (°C)
1	50	1086	200	200	12.70
2	30	1086	220	200	10.00
3	40	1086	210	200	10.41
4	50	837	200	200	8.43
5	50	750	200	200	7.27
6	50	650	200	200	5.42
7	50	550	200	200	6.07
8	50	600	200	200	4.65
9	50	610	200	200	4.38

As shown in Table IX, the total solidification cycle for the simulations was 250 seconds, which as previously mentioned was based on cycling the mold before the experimental trials began. The experimental solidification time as displayed in Figure 32 was 200 seconds. During the trials, the added vibration and a second person assisting reduced the cycle time of the mold, but the simulation time was not altered to match. Additionally, it is likely during the trials, the castings were being removed before full solidification was reached. This difference is unfortunate, but the same differences in HTC and temperatures should occur regardless.

Simulation with Three-step HTC Values

To further reduce the error value, four simulations were ran using a three-step HTC value. For the two-step simulation, the greatest increase in error occurred after the 50 second mark, so for the three step simulations a second HTC transition step was added after the initial 50 seconds. The second stage was varied from 20-50 seconds with all the simulated values shown in Figure 33 and the closest simulation highlighted in Figure 34. Once again, the average absolute error was calculated between Shot #22 temperatures and the simulated temperatures with the error values displayed in Table X. The simulation with the lowest error of 2.47°C used 610 $Wm^{-2}K^{-1}$ for the first 50 seconds followed by 400 $Wm^{-2}K^{-1}$ for the next 30 seconds and finally 100 $Wm^{-2}K^{-1}$ for the last 170 seconds. In summary, the lowest error value for a one step process was 7.17°C, 4.38°C for a two-step process, and 2.47°C for a three-step process. With each additional process step, the simulated temperature values became closer to the experimental value, but there was a reduction in error improvement. It seems feasible an additional fourth or fifth HTC step could reduce the error even more but the large reductions in error values would be unlikely.

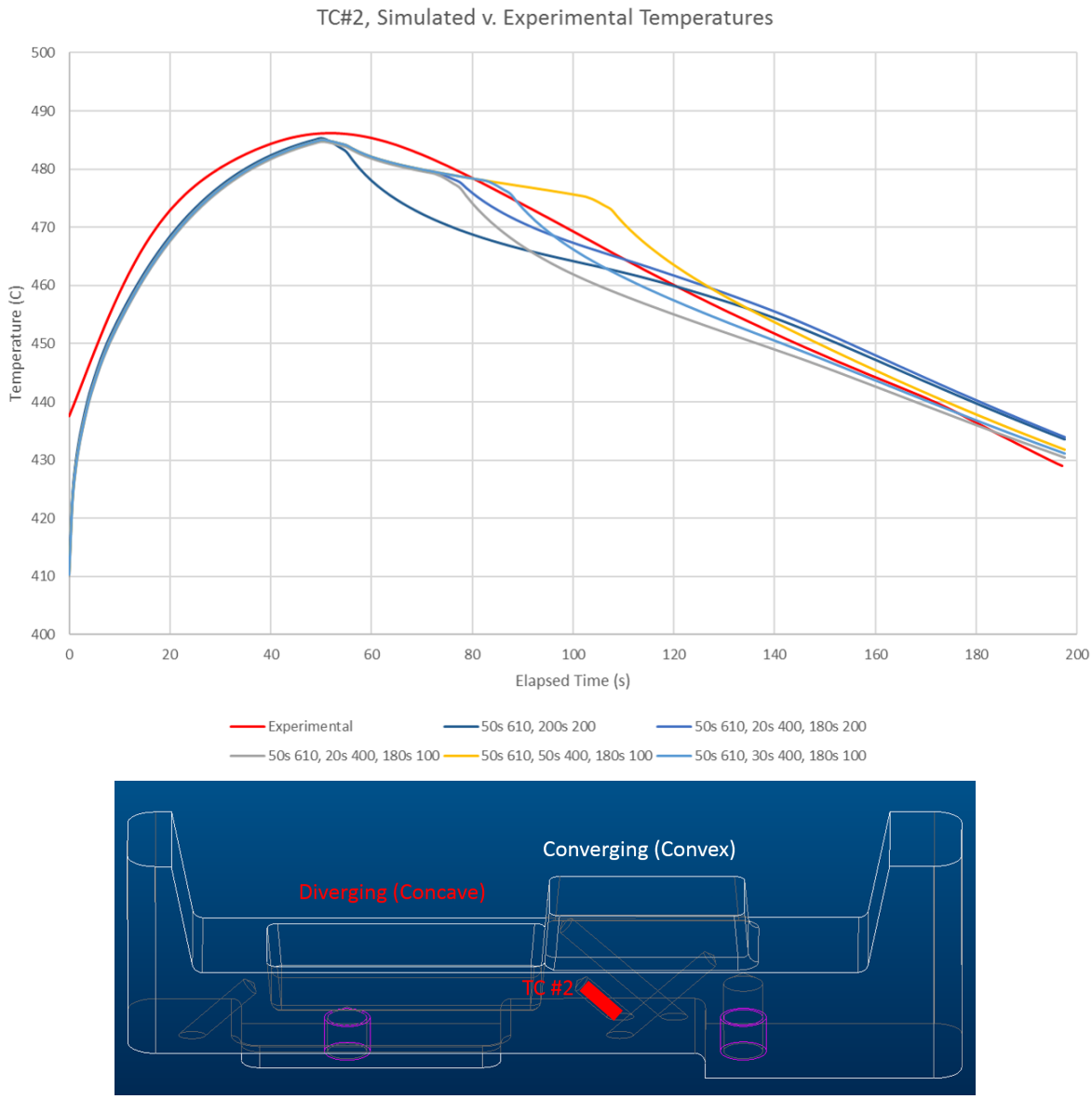

Figure 33: Linamar Mold: (Above) Shot #22 TCs #2 v. Three Step Simulation, (Below) Thermocouple Location.

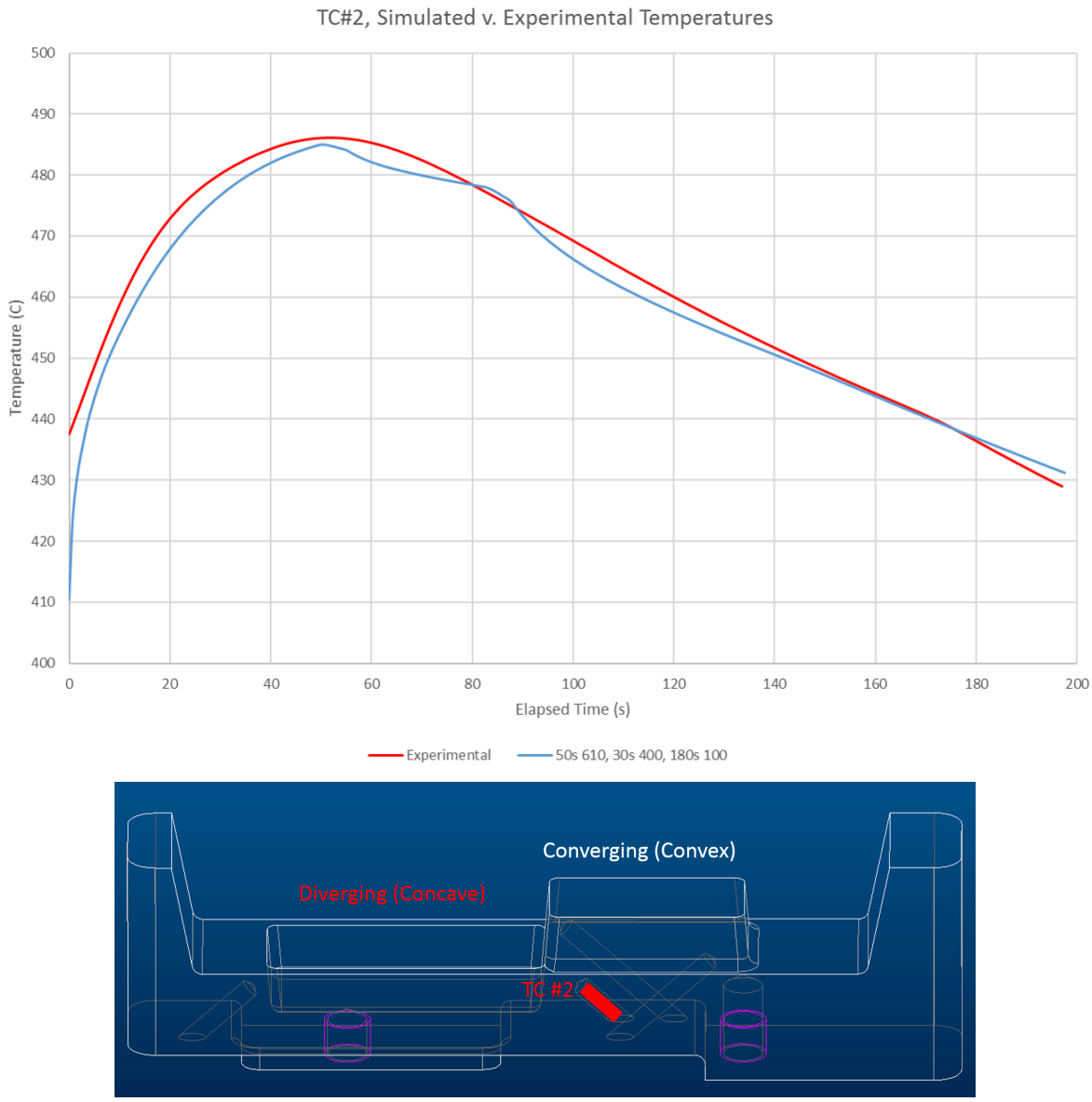

Figure 34: Linamar Mold: (Above) Shot #22 TCs #2 v. Simulation #9, (Below) Thermocouple Location.

Table X: Linamar Mold: Shot #22 TC#2 with Three Step HTC Value.

	Step 1		Step 2		Step 3		
Three Step Simulation	Time (s)	HTC (W/m^2.K)	Time (s)	HTC (W/m^2.K)	Time (s)	HTC (W/m^2.K)	Average Absolute Error (°C)
1	50	610	20	400	180	100	3.43
2	50	610	20	400	180	100	3.83
3	50	610	50	400	150	100	3.27
4	50	610	30	400	170	100	2.47

5.3 Influence of Geometry

Based on the results from the TC#2 simulations, the additional modeling for TC#3 was started using a three step HTC value with ten simulations ran in total as shown in Figure 35, and only the closest simulation displayed in Figure 36. The closest three-step HTC value was 1900 $Wm^{-2}K^{-1}$ for 50 seconds followed by 1000 $Wm^{-2}K^{-1}$ for the next 30 seconds and finishing with 400 $Wm^{-2}K^{-1}$ for the remaining 170 seconds. The average absolute error values for all the models are displayed in Table XI with the closest simulations having an error of 3.86°C. For comparison, the closest one step HTC error was 6.02°C. Initially during modeling, the HTC value for the first step was incrementally raised from 1086 to 1900 $Wm^{-2}K^{-1}$. As a starting point, the values for the second and third HTC stages from TC#2 simulations, 400 $Wm^{-2}K^{-1}$ for 30 second and 100 $Wm^{-2}K^{-1}$ for the final 170 seconds, were used but even with a higher Step 1 HTC value of 1850 $Wm^{-2}K^{-1}$ the absolute error was 10°C. To reduce the error, the second stage HTC value had to be increased from 400 to 1000 $Wm^{-2}K^{-1}$ while the third stage HTC value went from 100 to 400 $Wm^{-2}K^{-1}$.

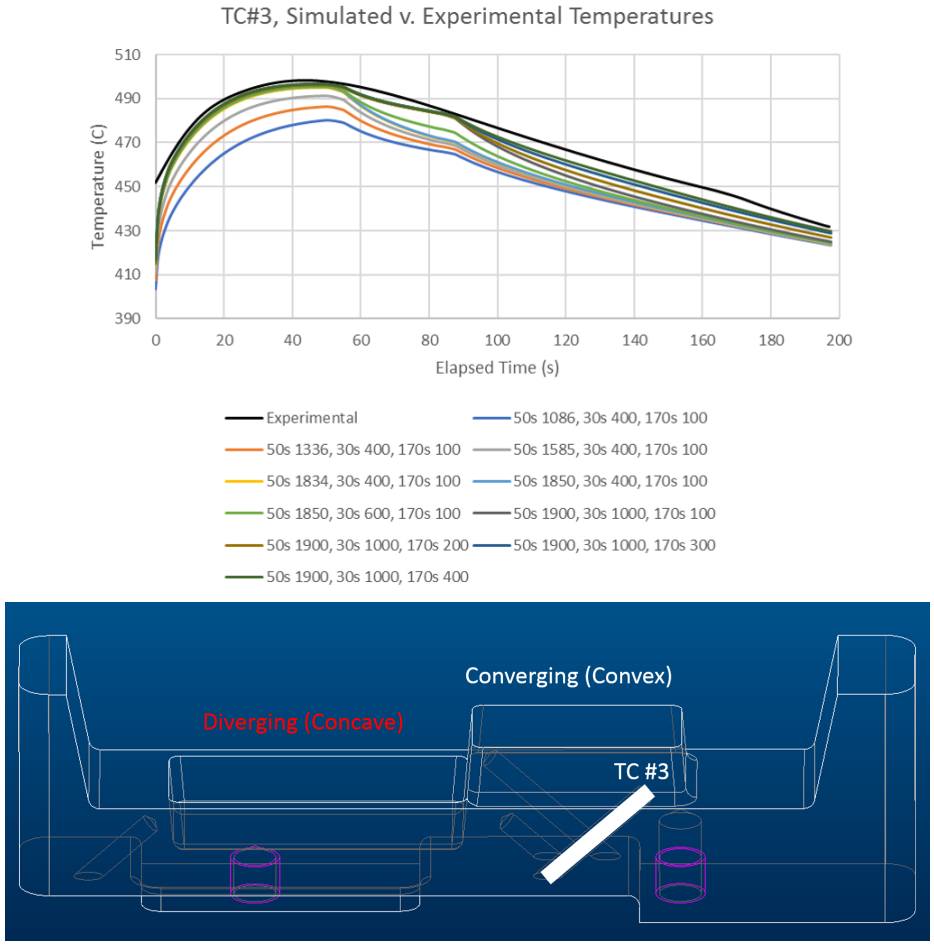

Figure 35: Linamar Mold: (Above) Shot #22 TCs #3 v. Three Step Simulation, (Below) Thermocouple Location.

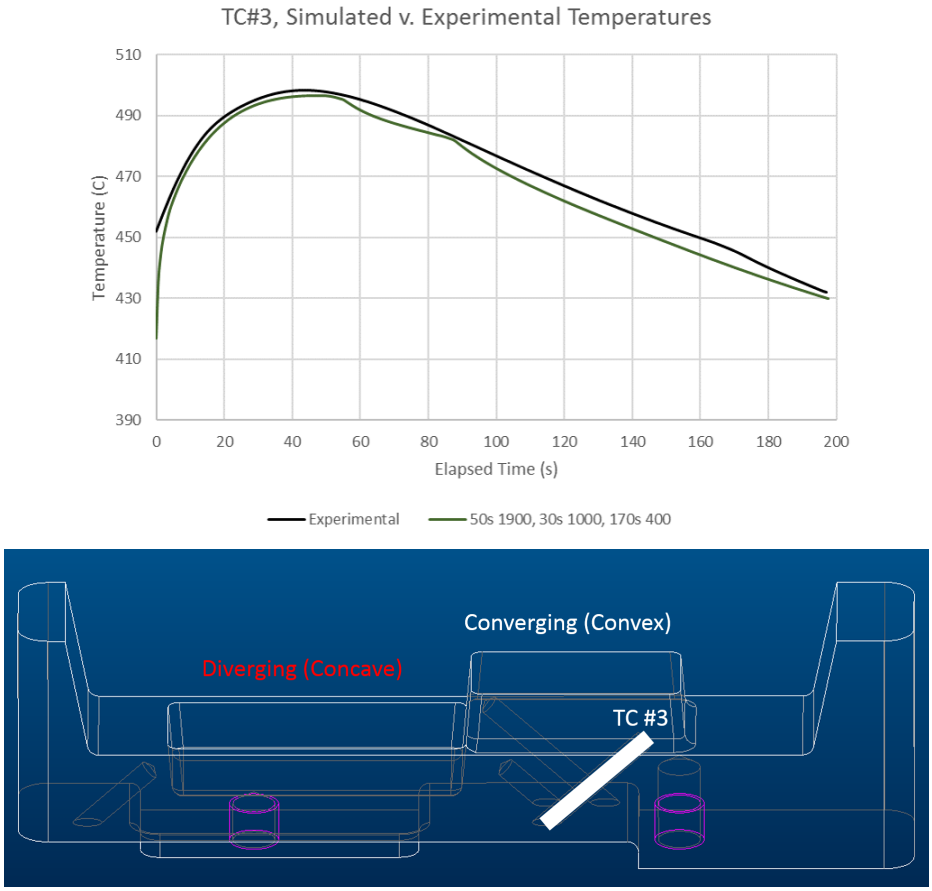

Figure 36: Linamar Mold: (Above) Shot #22 TC #3 v. Simulation #10, (Below) Thermocouple Location.

Table XI: Linamar Mold: Shot #22 TC#3 with Three Step HTC Value.

	Step 1		Step 2		Step 3		
Three Step Simulation	Time (s)	HTC (W/m^2.K)	Time (s)	HTC (W/m^2.K)	Time (s)	HTC (W/m^2.K)	Average Absolute Error (°C)
1	50	1086	30	400	170	100	18.89
2	50	1336	30	400	170	100	15.70
3	50	1585	30	400	170	100	13.14
4	50	1834	30	400	170	100	11.03
5	50	1850	30	400	170	100	10.90
6	50	1850	30	600	170	100	9.69
7	50	1900	30	1000	170	100	7.45
8	50	1900	30	1000	170	200	5.99
9	50	1900	30	1000	170	300	4.82
10	50	1900	30	1000	170	400	3.86

The formation of the air gap appears to occur at different rates for TCs #2 and #3 which is shown in Figure 37. When curves are overlapped without regards to temperature, TC #3 ascends more quickly and descends at a steeper angle but reaches the same temperature as TC #2 at the

end of the cycle. It appears there may be higher contact initially at the convex tooling feature transferring more heat, but there is a somewhat steeper drop as the air gap forms. Even with the steeper slopes, the HTC value during the air gap formation was much higher for TC #3.

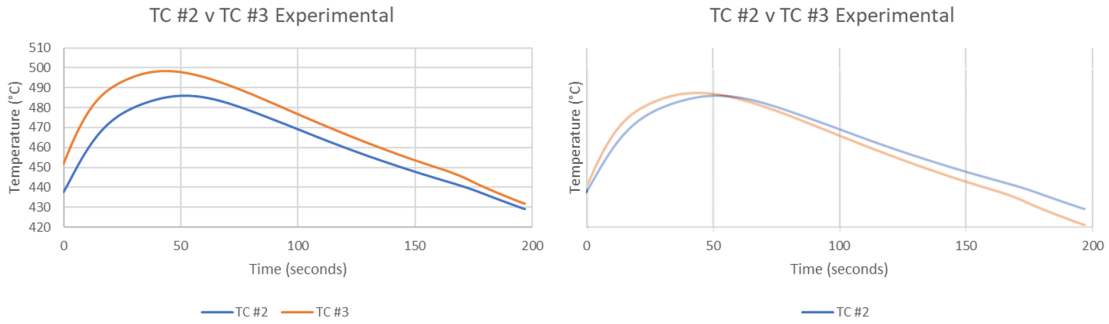

Figure 37: Linamar Mold: (Left) Shot #22 TCs #2 v. Simulation #3, (Right) TCs #2 and #3 slopes overlapped.

5.4 Influence of Mold Coating Wear

Temperatures

For a comparison between the new and worn standard coating, Shot #180 was selected as a steady temperature example as shown in Figure 38. Initially Shot #198 was selected but there were visual errors in the temperature readings for TC #2 (Figure 39). This error began at Shot #182, which is why Shot #180 was ultimately selected as an example of a casting cycle with a "worn" coating. Since five trials had been performed over several months and the testing apparatus was moved several times, it is likely thermocouple #2 became slightly dislodged causing a change in connection resulting in the inconsistent readings. Additionally, with each casting cycle the mold was opened while being subjected to vibration to remove the casting and closed again so the thermocouple endured notable movement.

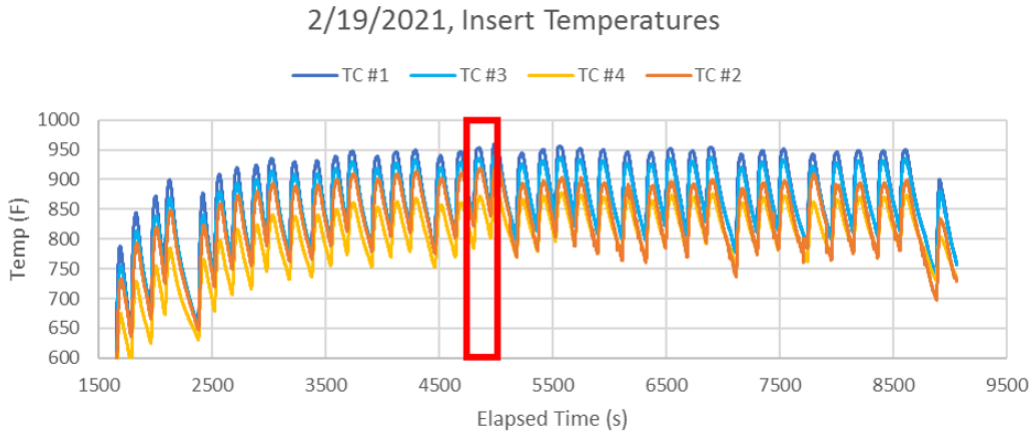

Figure 38: Linamar Mold: Trial #5 with Shot #180 highlighted in red.

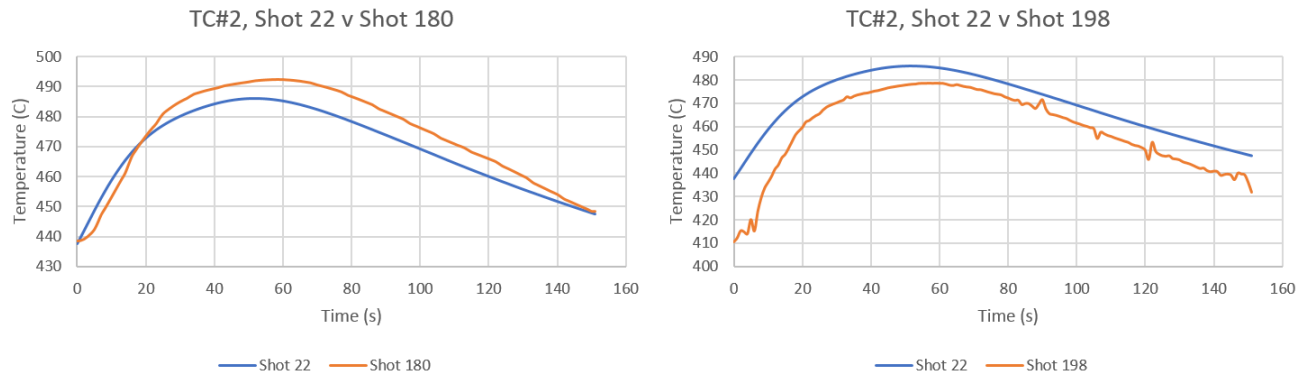

Figure 39: Linamar Mold: (Left) Shot #180 (Right) Shot #198 with error in Shot #2 Temperatures.

The difference between Shot #22 (new coating) and Shot #180 (worn coating) for both thermocouples #2 and #3 are shown in Figure 40. Visually, there were differences between the new and worn coating casting shots with the worn shot (#180) showing a steeper initial slope followed by a higher peak temperature. Based on the difference in temperatures, there was a higher amount of heat being transferred with the worn coating which results in the higher max temperatures and faster cooling. To remain consistent with the simulation discussion, average absolute error was used to compare the temperature differences between the worn and coating as measured by thermocouples #2 and #3. Thermocouple #2 showed an error value of 5.34°C but TC#3 had an error value of 3.98°C. These error values show mold coating wear caused a change in the temperature readings, but not a dramatic change.

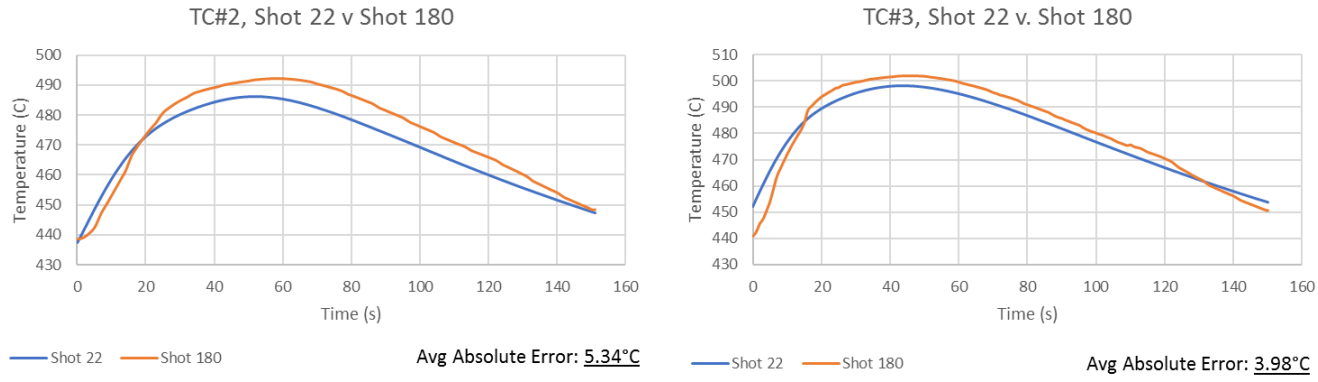

Figure 40: Linamar Mold: [Left] TC#2 New (Shot #22) v. Worn (Shot #180) Temperatures [Right] TC#3 New (Shot #22) v. Worn (Shot #180) Temperatures.

Mold Coating Measurements

As previously mentioned, mold coating wear was measured using an Elcometer at the end of each trial starting with Trial #2. A visual comparison of the coating wear is shown in Figure 41, which shows decrease in the outer graphite release coating and a gradual appearance of the brown middle coating layer. The coating wear measurements taken after each trial are shown in Table XII

and Figure 42. The thickness for the standard three-layer coating varied from 10-14 mils (0.254-0.356 mm) as applied with the middle brown coating existing between 7-8 mils (0.178-0.203 mm) cumulative. The total coating thickness after 200 casting shots measured 8.0 mils (0.203 mm) and 8.2 mils (0.208 mm), which puts it right at the edge of the middle brown layer. The simulated worn standard coating used in the fiber optic trials had a cumulative thickness of roughly 7 mils (0.178 mm) cumulative, so it would have been ideal to run the casting trials until 7 mils (0.178 mm) were reached but time was limited. It was exceedingly difficult to keep the coating measurement surface clear from over-spray, which is collateral spray when another area of the tooling was sprayed. There was some over-spray on the measurement area which can be seen in Figure 41B on the flat surface. A light blue boron nitride coating was applied to the base of the tool intermittently, and there is visually a small amount of blue on the measurement surface.

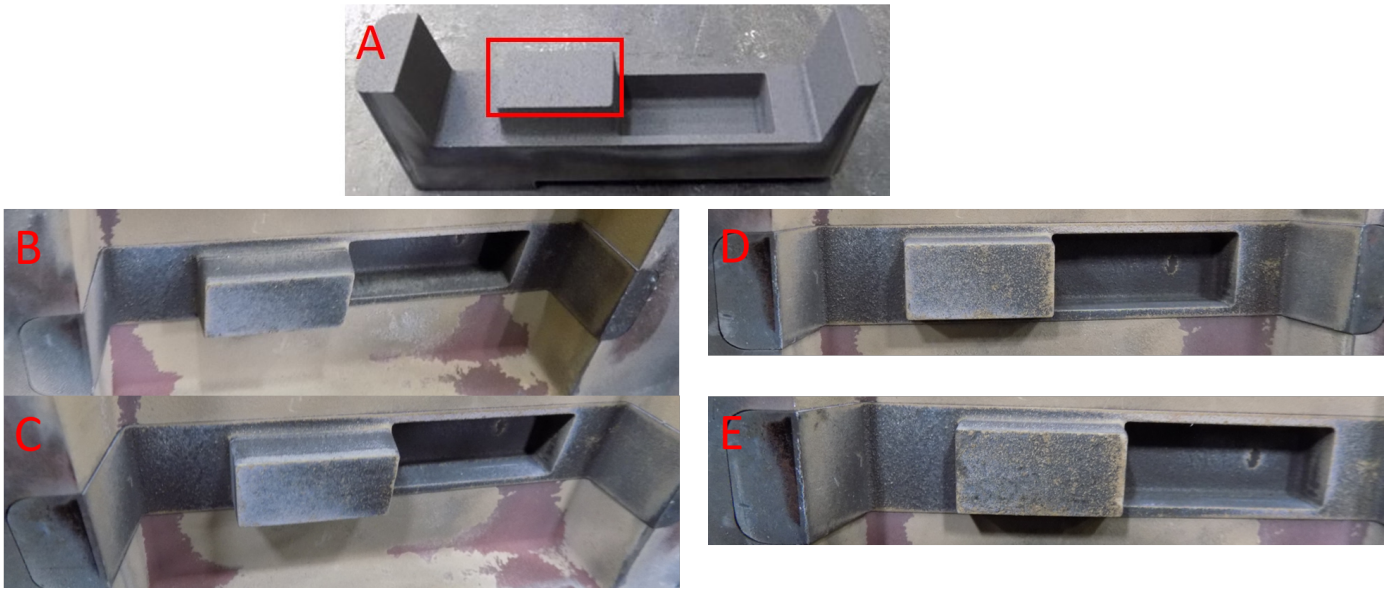

Figure 41: Linamar Mold: (A) Mold Coating at 0 castings shots, Measurement location highlighted in Red (B) Mold Coating at 64 casting shots (C) Mold Coating at 111 casting shots (D) Mold Coating at 162 casting Shots (E) Mold Coating at 200 casting shots.

Table XII: Linamar Mold: (Top) Coating Thickness Measurements in mils (Lower) Measurement Locations.

Trial	Date	Alloy	Casting Shots	Cumulative Casting Shots	Thickness, Location #1 (mils)	Thickness, Location #2 (mils)
1	10/30/2020	320	29	29	-	-
2	11/4/2020	320	35	64	10.8	12.3
3	1/13/2021	320	47	111	8.7	10.4
4	1/27/2021	A356	51	162	8.7	8.4
5	2/19/2021	320	38	200	8.0	8.2

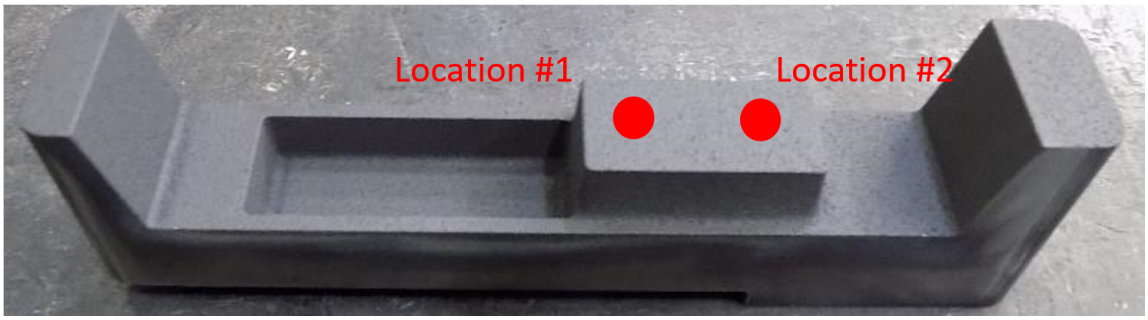

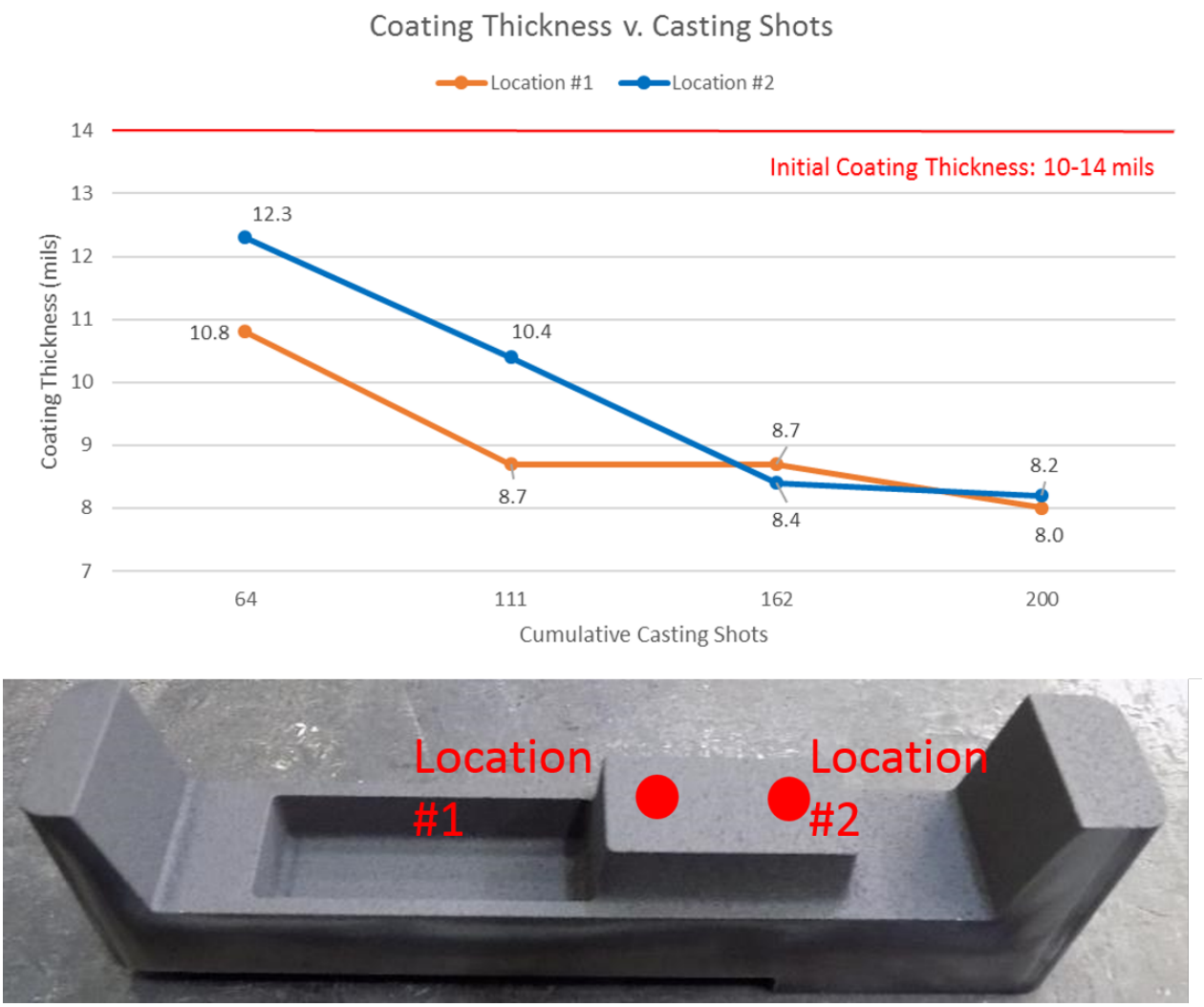

Figure 42: Linamar Mold: (Top) Coating Thickness v. Cumulative Shots (Lower) Measurement Locations.

Simulation Results

The temperature readings from thermocouples #2 and #3 recorded during Shot #180 were compared with the lowest error three step HTC simulation curves for Shot #22. As shown in Figure 43, the error for TC#2 was 12.85°C for the worn coating as compared to 2.47°C for the new coating (Shot #22). Thermocouple #3 showed a similar pattern with a 13.52°C error for the worn coating and 3.86°C for the new coating. To increase accuracy of casting simulations, new and worn coating scenarios need to be modeled, especially for applications where casting filling and/or feeding is difficult or marginals. The largest cause of the error between Shot #180 and the simulations for both thermocouples were the temperatures after the first 30 seconds which relate to the air gap formation. Past the 30 second mark, the worn coating experimental temperatures were higher for the rest of the cycle.

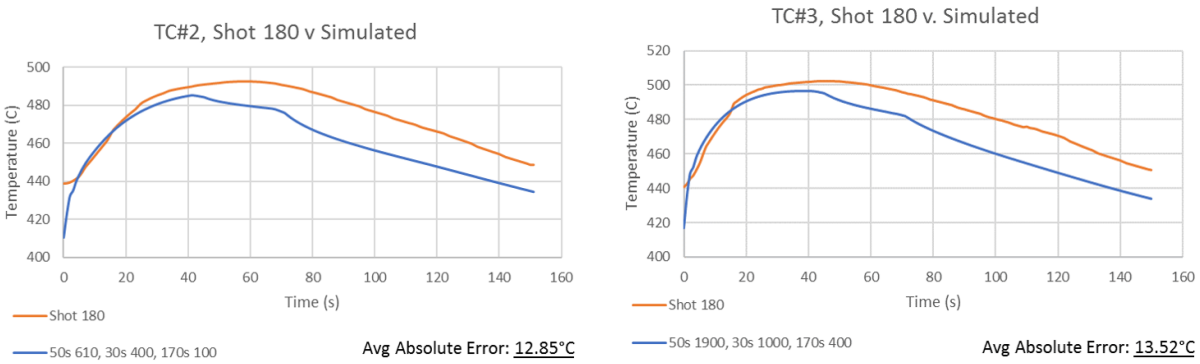

Figure 43: Linamar Mold: [Left] TC#2 Worn (Shot #180) v. Simulated Temperatures [Right] TC#3 Worn (Shot #180) v. Simulated Temperatures.

5.5 Fiber Optic Trials

While preheating the new coating fiber optic mold, the lower fiber optic cable was damaged and unable to accurately record temperatures. The fibers are exceptionally fine and translucent which makes them extremely difficult to see, but temperatures were successfully recorded using the top fiber optic cable (Figure 44). The locations along the fiber optic compared to the mold locations are displayed in Figure 45. While the fiber ran the length of the mold, one section of the casting (Left Middle to Left Outer Wedge) did not completely stay in contact with the top fibers which is shown in Figure 46.

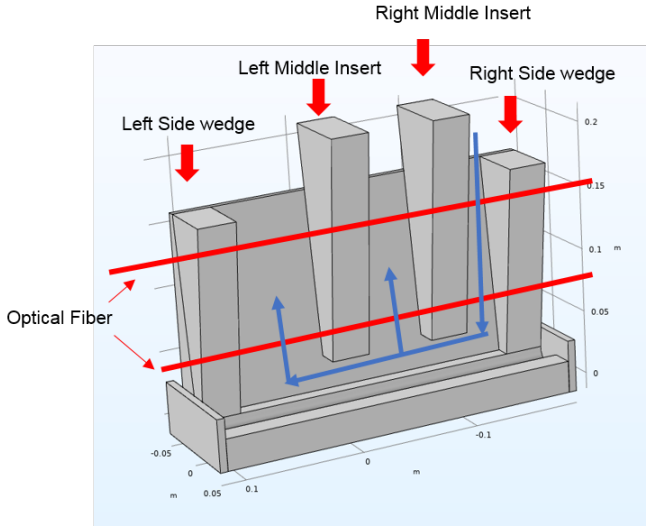

Figure 44: ACRC Wedge Mold: Top and Lower Optical Fiber positions in Wedge Mold with blue arrows indicating metal flow direction during mold filling.

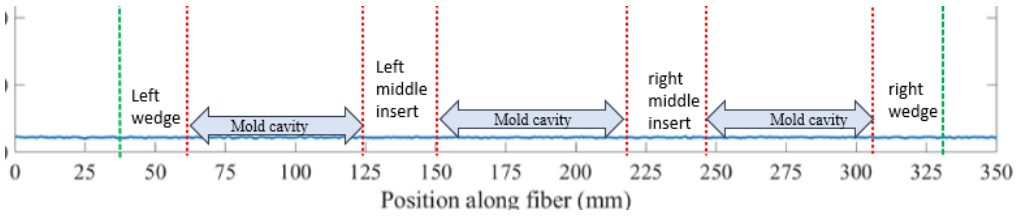

Figure 45: ACRC Wedge Mold: Position of Fiber with relation to Mold Inserts.

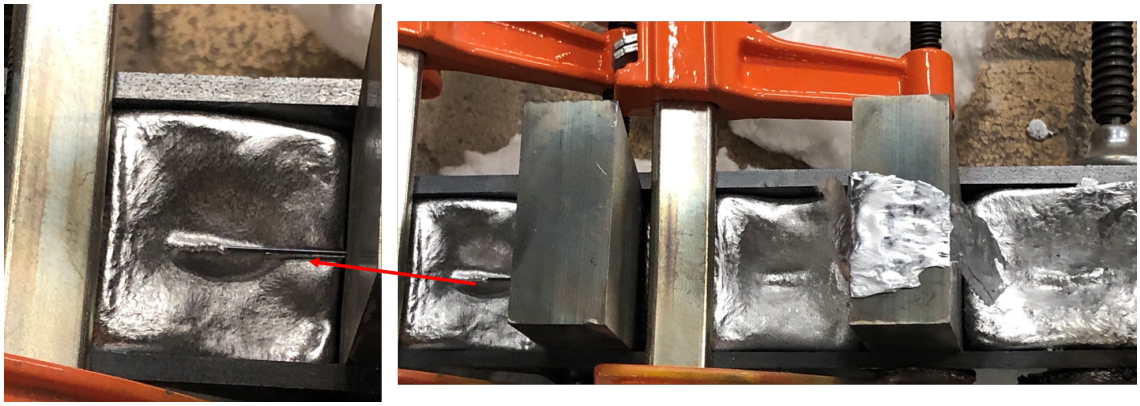

Figure 46: ACRC Wedge Mold: Fiber Exposed to Air (Highlighted in Red).

With the fiber optic trials, one of the primary purposes was to make a direct comparison with the inserted thermocouple readings in the Linamar mold. As mentioned previously thermocouples #2 and #3 in the Linamar mold were used to compare heat transfer coefficients, which are both 6.35 mm (0.25") from the castings. While temperatures were recorded along the entire length of the top fiber optic cable in 0.65 mm increments, only temperatures roughly 6 mm away from the casting surface were used to make a direct comparison to the Linamar mold with temperatures for the left outer, left middle, right middle, and right outer wedges shown in Figure 47.

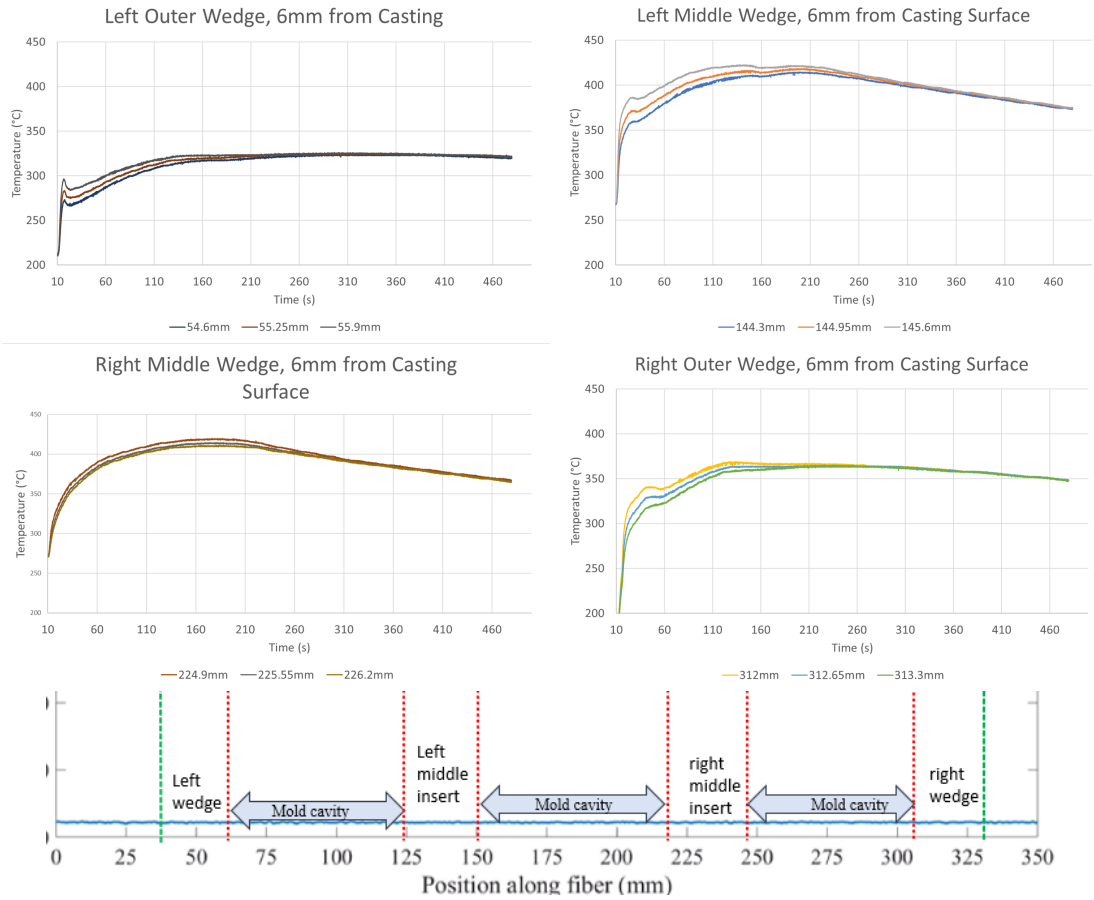

Figure 47: ACRC Wedge Mold: (Top Left) Left Outer Wedge (Top Right) Left Middle Wedge (Middle Left) Right Middle Wedge (Middle Right) Right Outer Wedge (Bottom) Position of Fiber Optic in Mold.

From analyzing the wedge temperatures 6mm from the casting surface, there is a distinct difference in the temperature pattern for the outer and inner wedges. The outer wedges reach a sharp peak from 300-330°C followed by a max temperature at 120 seconds between 320-360°C with extraordinarily little temperature drop off for the rest of the cycle. The middle wedges show a much more gradual increase in temperature like the Linamar mold, but a max temperature of roughly 410°C reached at 160 seconds. The max temperature follows a steeper decline in temperature as compare to the outer wedges; overall the inner wedges are more like thermocouples #2 and #3 in the Linamar mold. The difference between the outer and inner wedges was the inner wedges were surround on both sides by heat sources (aluminum casting), while the outer wedges had ambient air on one side. This is the most likely reason that the outer wedges never reached the same peak temperatures and did not show a corresponding dip in temperature.

A direct comparison is made between Right Middle Wedge temperature and thermocouple #2 from Shot #22 for the experimental temperature are shown in Figure 49. In general, the shape of the temperature curves is remarkably similar between the middle wedge and thermocouple #2, but with two main differences. The overall temperature cycle was much longer for the Wedge trial (460 seconds) than for the Linamar trial (200 seconds). Second the Linamar trial thermocouple

#2 (490°C) had an 80°C higher max temperature as compared to the middle insert (410°C). Some of the max temperature difference was due to the pouring temperature for both trials with 720°C used for the Wedge Mold Trial and 743°C for the Linamar Trial or a difference of 23°C. This does not account for the entire difference in temperatures, but the Linamar trial was run with multiple shots and a steady temperature was reached, while the Wedge mold was only single casting shot, so the starting mold temperature was much higher for the Linamar mold. Additionally, since multiple Linamar casting were made, the mold was cycled as soon as a casting could be removed which accounts for the much shorter cycle times.

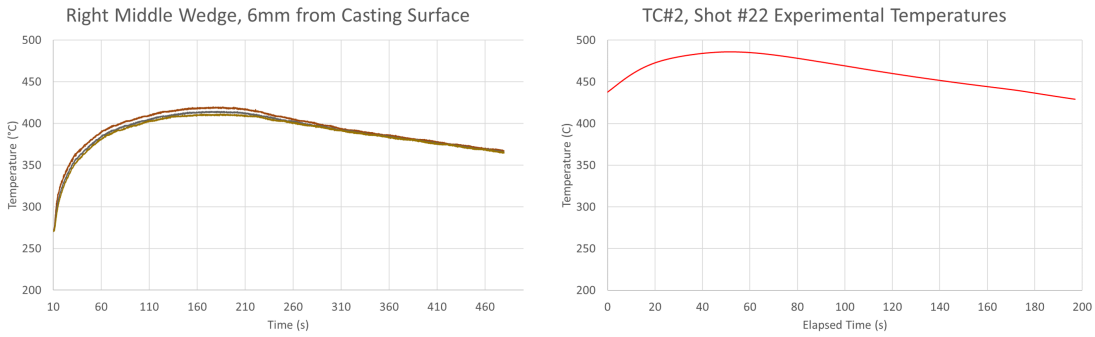

Figure 48: ACRC Wedge Mold: (Left) Right Middle Wedge Temperature (Right) Linamar Shot #22 Thermocouple #2.

A comparison between Right Middle Wedge and the simulated Thermocouple #2 temperature is shown in Figure 48. Obviously, the simulated and experimental temperatures for thermocouple #2 were remarkably close with a general pattern followed, but the simulated temperature always showed a much sharper initial increase in temperature than was shown in the experimental data. A similar initial sharp increase in temperature is shown in the Right Middle Wedge temperature. The slight difference is most likely caused from the fiber optic reading being lower mass and faster response time to changes in temperature than the inserted thermocouple.

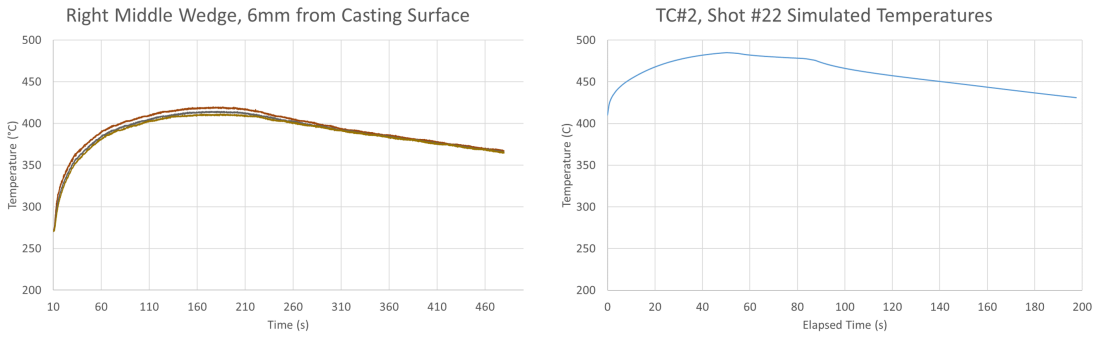

Figure 49: ACRC Wedge Mold: (Left) Right Middle Wedge Temperature (Right) Thermocouple #2 Simulated Temperature.

6 Conclusions

6.1 HTC - Critical Input Parameter

Based on experimental results with the Linamar mold, heat transfer coefficient (HTC) is a critical parameter in order to accurately simulate permanent mold casting temperatures. The simulated temperatures were easily manipulated with changes to the heat transfer coefficient. As mentioned in the literature review, heat transfer in permanent mold castings is primarily controlled by the resistance to heat transfer at the metal mold interface, so it is logical that heat transfer coefficient, which represents this interface, be critical parameter in solidification modeling. Using commercial software with built in HTC values that have not been verified may lead to variations between experimental or commercial results and those obtained by the software. It is imperative that the HTC values incorporated in commercial software be verified and validated.

6.2 HTC Multiple Step Values

In addition to HTC being critical to accurate simulations, a single heat transfer value for the entire solidification cycle is not an accurate way to simulate permanent mold castings. As shown with the error values produced in the one-step, two-step, and three-step HTC values, simulated temperatures become more accurate as heat transfer coefficients changed with time. The primary reason for the transitive nature of the heat transfer coefficient is the formation of an air gap between the casting and mold surfaces, which drastically reduces heat transfer. Due to this air gap, heat transfer values peaked at roughly 50 seconds and decreased as the air gap forms. A single step HTC value will yield results which do not simulate reality. HTC needs to be represented as a function of time that considers the air gap formation.

6.3 Geometry Influence on HTC

Aside from the formation of an air gap, geometry is another factor which impacts the heat transfer coefficient as shown by the temperature difference between thermocouples #2 and #3 in the Linamar mold. Thermocouple #2 was representative of a concave tooling surface while thermocouple #3 measured a convex tooling surface, which were both 6.35 mm (0.25”) from the casting surface, respectively. With regards to simulations, the convex surface required almost double the HTC as compared to the concave surface. The convex surface caused a faster initial increase in temperature followed by a quicker decline in temperature. This was due to the increased casting to mold surface contact from the difference in geometry.

6.4 Coating Wear Influence on HTC

In addition to geometry, mold coating wear impact heat transfer coefficient (HTC) in aluminum permanent mold castings as shown by the temperature difference between Shot #22 and Shot #180. As the coating thickness decreased from approximately 14 mils (0.356 mm) to 8 mils (0.203 mm), the temperature readings changed with a steeper initial increase in temperature followed by a higher max temperature. As the coating wears, it becomes smoother and thinner which reduces the amount of air gaps at the mold interface and make the coating less insulating. This change in HTC due to

the coating wear makes accurately simulating a casting even more difficult. Since HTC becomes a moving target as the coating wears; casting simulations should be simulated with a new coating and a worn coating. The function of HTC with time needs to be considered; air gap, geometry, and coating thickness cannot be neglected.

6.5 Temperature Measurements using Fiber Optics

The inserted fiber optics were proven to be an accurate method to measure temperatures within a permanent mold. The inner wedge temperatures at 6.35 mm displayed the same general curves as thermocouples #2 and #3, which were also at a similar depth. The curves showed a fast increase in temperature until a max temperature was reached followed by a gradual decline caused by the development of an air gap. The Linamar mold temperatures were higher, but this was due to a higher furnace temperature and shorter mold cycle time, which led to higher mold temperatures. Moreover, the inserted fiber optic could measure the initial increase in temperature as seen in the simulations, which were not shown with the inserted thermocouples. The viability and feasibility of the use of fiber optics to measure HTC has be validated.

7 Recommendations for Further Work

While the Linamar experiments showed heat transfer coefficient changes based on coating wear, the amount of wear did not achieve the same severity as that experienced by the industrial trials. With the setup that was used in this study, it was not feasible to run the mold for long times (more than 5 hours). We recommend a mold designed for production trials that would have been able to produce castings more efficiently and could have reduces the time require for trials.

Additionally, we recommend a production tool would have an in-built ejector system to prevent the casting from hanging up in the tool. To further measure effect geometry and pressure differences on heat transfer coefficient, the new tool design could include a cope, drag, and two wall sides. The convex and concave geometries would be repeated in the cope, drag, and sides which should experience different pressures from mold location resulting in different heat transfer values. It would be novel to measure differences in part geometry in addition to pressure difference due to mold location.

In terms of information gained from current production tooling, mold coating thickness could be measured with a variety of production tools which would give a more complete insight into the extent of coating thickness as applied and as through wear during normal production. This production information could also be to define coating thickness as a function of time. Furthermore, existing production castings, which do not accurately match simulations, could be used as examples to test the effectiveness of multistage heat transfer coefficient simulations.

Most importantly, this work has shown the criticality of HTC for accurate solidification simulations. We recommend a focused study to measure HTC in-situ and have the “true and instantaneous” HTC be incorporated in simulations as a function of time, which would likely incorporate the use of fiber optics. While the use of fiber optics was only briefly investigated within this research, their possible application for the improvement of solidification modeling is great, especially given their ability to calculate heat transfer coefficient using a single fiber with the Inverse method. Also, there exists the possibility to improve simulation accuracy by relating heat transfer coefficient to critical

temperatures such as solidus point, liquidus point, dendrite coherency temperature, and interface temperature.

8 References

[1] John L Jorstad and Wayne M Rasmussen. *Aluminum casting technology*. Amer Foundry Society, 1993.

[2] John Campbell. *Complete casting handbook: metal casting processes, metallurgy, techniques and design*. Butterworth-Heinemann, 2015.

[3] Merton C Flemings. "Solidification processing". In: *Metallurgical transactions* 5.10 (1974), pp. 2121–2134.

[4] Mervin T Rowley. *International atlas of casting defects*. American Foundrymen's Society, 1993.

[5] Joy A Hines. "Determination of interfacial heat-transfer boundary conditions in an aluminum low-pressure permanent mold test casting". In: *Metallurgical and materials transactions B* 35.2 (2004), pp. 299–311.

[6] R Viskanta. "Heat transfer during melting and solidification of metals". In: (1988).

[7] WD Griffiths. "A model of the interfacial heat-transfer coefficient during unidirectional solidification of an aluminum alloy". In: *Metallurgical and Materials Transactions B* 31.2 (2000), pp. 285–295.

[8] Yin-Heng Chen and Yong-Taek Im. "Analysis of solidification in sand and permanent mold castings and shrinkage prediction". In: *International Journal of Machine Tools and Manufacture* 30.2 (1990), pp. 175–189.

[9] Kuang-Oscar Yu. *Modeling for casting and solidification processing*. CRC Press, 2001.

[10] Doru Michael Stefanescu. *Science and engineering of casting solidification*. Springer, 2015.

[11] VE Bazhenov, Yu V Tselovalnik, AV Koltygin, and VD Belov. "Investigation of the Interfacial Heat Transfer Coefficient at the Metal–Mold Interface During Casting of an A356 Aluminum Alloy and AZ81 Magnesium Alloy into Steel and Graphite Molds". In: *International Journal of Metalcasting* (2020), pp. 1–13.

[12] Adrian S Sabau. "Heat Fluxes at Metal-Mold Interface During Casting Solidification". In: *LIGHT METALS-WARRENDALE-PROCEEDINGS-*. TMS, p. 827.

[13] Ruey-Jer Weng, Jer-Haur Kuo, Weng-Sing Hwang, Jean-Francois Moisan, and Cheng-Kuei Jen. "JGGGG S0JGS". In: *Proceedings of the International Conference on Solidification Processing*. Vol. 2. 2007, pp. 07–25.

[14] SN Kulkarni and K Radhakrishna. "Evaluation of metal–mould interfacial heat transfer during the solidification of aluminium–4.5 copper alloy castings cast in CO2–sand moulds". In: *Materials Science-Poland* 23.3 (2005), pp. 821–838.

[15] Yukinobu Natsume, Yukimi Oka, Jota Ogawa, and Munekazu Ohno. "Estimation of time-dependent heat transfer coefficient in unidirectional casting using a numerical model coupled with solidification analysis and data assimilation". In: *International Journal of Heat and Mass Transfer* 150 (2020), p. 119222.

[16] A Fardi Ilkhchy, Masoud Jabbari, and P Davami. “Effect of pressure on heat transfer coefficient at the metal/mold interface of A356 aluminum alloy”. In: *International Communications in Heat and Mass Transfer* 39.5 (2012), pp. 705–712.

[17] Gilles Dour, Matthew Dargusch, Cameron Davidson, and A Nef. “Development of a non-intrusive heat transfer coefficient gauge and its application to high pressure die casting: effect of the process parameters”. In: *Journal of Materials Processing Technology* 169.2 (2005), pp. 223–233.

[18] Muhammad Roman, Damilola Balogun, Yiyang Zhuang, Rex E Gerald, Laura Bartlett, Ronald J O’Malley, and Jie Huang. “A spatially distributed fiber-optic temperature sensor for applications in the steel industry”. In: *Sensors* 20.14 (2020), p. 3900.

[19] RD Pehlke and SW Hao. “Heat transfer at the mold-metal interface in permanent mold casting of aluminum alloys project”. In: *Ann Arbor* 1001 (1998), pp. 48109–2136.

[20] Dirk Lieftucht, Markus Reifferscheid, Thomas Schramm, Artemy Krasilnikov, and Dieter Kirsch. “HD Mold–A new Fiber-Optical-based Mold Monitoring System”. In: *Iron and Steel Technology* (2013), pp. 87–95.

[21] Bowei Zhang and Mojtaba Kahrizi. “High-temperature resistance fiber Bragg grating temperature sensor fabrication”. In: *IEEE sensors journal* 7.4 (2007), pp. 586–591.

[22] MA Taha, NA El-Mahallawy, MT El-Mestekawi, and AA Hassan. “Estimation of air gap and heat transfer coefficient at different faces of Al and Al–Si castings solidifying in permanent mould”. In: *Materials science and technology* 17.9 (2001), pp. 1093–1101.

[23] Basil Coates and Stavros A Argyropoulos. “The effects of surface roughness and metal temperature on the heat-transfer coefficient at the metal mold interface”. In: *Metallurgical and Materials Transactions B* 38.2 (2007), pp. 243–255.

[24] Ivaldo L Ferreira, Jose E Spinelli, Jose C Pires, and Amauri Garcia. “The effect of melt temperature profile on the transient metal/mold heat transfer coefficient during solidification”. In: *Materials Science and Engineering: A* 408.1-2 (2005), pp. 317–325.

[25] Jer-Haur Kuo, Ruey-Jer Weng, and Weng-Sing Hwang. “Effects of solid fraction on the heat transfer coefficient at the casting/mold interface for permanent mold casting of AZ91D magnesium alloy”. In: *Materials transactions* 47.10 (2006), pp. 2547–2554.

[26] Anwar Hamasaiid, MS Dargusch, CJ Davidson, S Tovar, Tahar Loulou, Farhad Rezai-Aria, and Gilles Dour. “Effect of mold coating materials and thickness on heat transfer in permanent mold casting of aluminum alloys”. In: *Metallurgical and materials Transactions A* 38.6 (2007), pp. 1303–1316.

[27] Matthew S Dargusch, Anwar Hamasaiid, Gilles Dour, Tahar Loulou, Cameron J Davidson, and David H StJohn. “The Accurate Determination of Heat Transfer Coefficient and Its Evolution With Time During High Pressure Die Casting of Al-9 Si-3 Cu and Mg-9 Al-1 Zn Alloys”. In: *Advanced Engineering Materials* 9.11 (2007), pp. 995–999.

[28] AM Assar. “Mould surface roughness and interfacial heat transfer using heat flow model”. In: *Materials science and technology* 13.8 (1997), pp. 702–704.

[29] VE Bazhenov, AV Koltygin, Yu V Tselovalnik, and AV Sannikov. “Determination of interface heat transfer coefficient between aluminum casting and graphite mold”. In: *Russian Journal of Non-Ferrous Metals* 58.2 (2017), pp. 114–123.

[30] K Narayan Prabhu and KM Suresha. “Effect of superheat, mold, and casting materials on the metal/mold interfacial heat transfer during solidification in graphite-lined permanent molds”. In: *Journal of Materials Engineering and Performance* 13.5 (2004), pp. 619–626.

[31] Anwar Hamasaiid, MS Dargusch, and Gilles Dour. “The impact of the casting thickness on the interfacial heat transfer and solidification of the casting during permanent mold casting of an A356 alloy”. In: *Journal of Manufacturing Processes* 47 (2019), pp. 229–237.

[32] Paal Schmidt. “Heat transfer during filling in die casting processes”. In: *Materials Science and Engineering: A* 173.1-2 (1993), pp. 271–274.

[33] Zhi-Peng Guo, Shou-Mei Xiong, Bai-Cheng Liu, Mei Li, and John Allison. “Effect of process parameters, casting thickness, and alloys on the interfacial heat-transfer coefficient in the high-pressure die-casting process”. In: *Metallurgical and Materials Transactions A* 39.12 (2008), p. 2896.

[34] Jacob O Aweda and Michael B Adeyemi. “Experimental determination of heat transfer coefficients during squeeze casting of aluminium”. In: *Journal of Materials Processing Technology* 209.3 (2009), pp. 1477–1483.

[35] Jia-hua Lin, Hai-dong Zhao, and Jia-min Huang. “Spatial interfacial heat transfer and surface characteristics during gravity casting of A356 alloy”. In: *Transactions of Nonferrous Metals Society of China* 29.1 (2019), pp. 43–50.

[36] WD Griffiths, K Narayan Prabhu, CP Hallam, and R Kayikci. “The deformation of the chill in experiments to determine the interfacial heat transfer coefficient during casting solidification”. In: *International Journal of Cast Metals Research* 15.5 (2003), pp. 545–550.

[37] N Akar, H Mehmet Sahin, N Yacin, and K Kocatepe. “Experimental study on the effect of liquid metal superheat and casting height on interfacial heat transfer coefficient”. In: *Experimental heat transfer* 21.1 (2008), pp. 83–98.

[38] Felipe Bertelli, Crystopher Brito, Elisangela S Meza, Noé Cheung, and Amauri Garcia. “Inward and outward solidification of cylindrical castings: The role of the metal/mold heat transfer coefficient”. In: *Materials Chemistry and Physics* 136.2-3 (2012), pp. 545–554.

[39] Jenny Kron, Michel Bellet, Andreas Ludwig, Bjorn Pustal, Joachim Wendt, and Hasse Fredriksson. “Comparison of numerical simulation models for predicting temperature in solidification analysis with reference to air gap formation”. In: *International Journal of Cast Metals Research* 17.5 (2004), pp. 295–310.

[40] Patrice Vicente-Hernandez, Florent Decultieux, Pål Schmidt, Ingvar L Svensson, and Christophe Levaillant. “Mushy state behavior: rheological characterization and influence on air gap formation”. In: *ISIJ international* 35.6 (1995), pp. 805–812.

[41] M Ahmadein, B Pustal, N Wolff, and A Buhrig-Polaczek. “Determination and verification of the gap dependent heat transfer coefficient during permanent mold casting of A356 aluminum alloy”. In: *Materialwissenschaft und Werkstofftechnik* 48.12 (2017), pp. 1249–1256.

[42] Yi Dan Zeng, Qing Hu Yao, and Xia Wang. “The Effect of Air Gap between Casting and Water-Cooled Mold on Interface Heat Transfer Coefficient”. In: *Materials Science Forum*. Vol. 893. Trans Tech Publ. 2017, pp. 174–180.

[43] Stavros A Argyropoulos and Horazio Carletti. “Comparisons of the Effects of Air and Helium on Heat transfer at the Metal-Mold Interface”. In: *Metallurgical and Materials Transactions B* 39.3 (2008), pp. 457–468.

[44] Eli Vandersluis and Comondore Ravindran. “Estimating the effective metal-mould interfacial heat transfer coefficient via experimental-simulated cooling curve convergence”. In: *Transactions of the Indian Institute of Metals* 71.5 (2018), pp. 1231–1236.

[45] Kamil Kunt Tuzunalp and Semsettin Ozdemir. “A geometry-based model for determining solidification isotherms of basic casting sections”. In: *Materials Chemistry and Physics* 233 (2019), pp. 27–45.

[46] B Zhang, DM Maijer, and SL Cockcroft. “Development of a 3-D thermal model of the low-pressure die-cast (LPDC) process of A356 aluminum alloy wheels”. In: *Materials Science and Engineering: A* 464.1-2 (2007), pp. 295–305.

[47] Joseph Ha, Paul Cleary, Vladimir Alguine, and Thang Nguyen. “Simulation of die filling in gravity die casting using SPH and MAGMAsoft”. In: *Proc. 2nd Int. Conf. on CFD in Mineralsand Process Industries*. 1999, pp. 423–428.

[48] Jer-Haur Kuo, Feng-Lin Hsu, and Weng-Sing Hwang. “Development of an interactive simulation system for the determination of the pressure-time relationship during the filling in a low pressure casting process”. In: *Science and Technology of Advanced Materials* 2.1 (2001), pp. 131–145.

[49] Yiu Wing Chan. “Application of a solidification model to the casting of an aluminium brake drum”. In: *Journal of Materials Processing Technology* 29.1-3 (1992), pp. 223–234.

[50] ASM International Handbook Committee et al. *Metals Handbook: Vol. 2, Properties and selection–nonferrous alloys and pure metals*. 1990.

[51] ASM International Handbook Committee et al. *ASM Handbook, Volume 15-Casting*. ASM International., 2008.